ADDIS ABABA UNIVERSITY
ADDIS ABABA INSTITUTE OF TECHNOLOGY
SCHOOL OF CIVIL AND ENVIRONMENTAL ENGINEERING

Regional Gravity Field Modelling From GRACE Satellite Gravity Mission Data: A Case Study in Ethiopia

A Thesis in Geodesy and Geomatics (specialization in Geodesy)

By Samuel Milki Yadeta

February 2022

Addis Ababa

A Thesis

Submitted in Partial Fulfillment of the Requirements for the Degree of Master Science

Approval Sheet

The undersigned have examined the thesis entitled 'Regional Gravity Field Modelling from GRACE Satellite Gravity Mission Data: A Case Study in Ethiopia' presented by Samuel Milki, a candidate for the degree of Master of Science, and hereby certify that it is worthy of acceptance.

Tulu Besha Bedada (Ph.D.) Advisor	Signature	21.04.2022 Date
Sintayehu A. Internal Examiner	Signature	21/04/2022 Date
Walyeldeen Godah (A/Prof.) External Examiner	Signature	16.04.2022 Date
Chair Person	Mebruk Mohammed (Dr.-Ing.) Dean, Sci :: vil & Environmental Engineering Signature	Date

Addis Ababa Institute of Technology
Director of Postgraduate Program
Addis Ababa University

Undertaking

I certify that this research work, with the title “Regional Gravity Field Modelling from GRACE Satellite Gravity Mission Data: A Case Study in Ethiopia” is my work. The thesis has not been submitted to anybody else for assessment. Where material has been used from other sources, it has been properly acknowledged/referred.

Signature of the Student

Samuel Milki Yadeta
Name of the Student

Abstract

The Gravity Recovery and Climate Experiment (GRACE) mission data-derived gravity field models have provided us with remarkable accuracy in gravity field determination. Despite this, the predicted GRACE baseline accuracy has yet to be met. One reason, among many, could be insufficient satellite data modeling using a global representation by Spherical Harmonics (SH). It appears appropriate to improve global solutions through regional recovery strategies to fully recover the signal information included in satellite and sensor data. Varied geographical regions have different gravity field characteristics, especially in the higher frequency part of the spectrum. As a result, the recovery process should be tailored to the specific characteristics of the area. This regional refinement strategy was employed in Ethiopia. Global gravity reference field, which is represented by SH expansion is then refined using regionally tailored refinements that are specified as space localizing basis functions using splines. The shape coefficients are obtained using the global gravity model's degree error variances truncated up to a maximum degree of 120. This means that the spline kernels must be adjusted to the spectral range of the gravity field features to be calculated. In addition, the raw accelerometer data measured by GRACE Satellites using onboard accelerometers was calibrated. Every short arc over the study area is used, with a 10° strip added to the recovery area. After being synchronized, these short arcs created a partial system of normal equations using an integral equation of the Fredholm type. These normal equations are accumulated to account for varied accuracies of short arcs by estimating variance factors for each arc using variance component estimation (VCE). For only one month of data collected in January 2016, the normal equations are solved using the least squares regularized approach. In the case of regularization, the regularization parameter was calculated using the same VCE method. Finally, the study area's regional refinement was determined a using geographic grid of $0.5° \, x 0.5°$ at sea level in Ethiopia. In terms of gravity anomaly and geoid height, the regional solution improves the Global gravity reference field in root mean square (rms) from $5.95 mGal$ to $4.33 mGal$ and $52.90 cm$ to $46.13 cm$ respectively.

Keywords: GRACE, Regional Gravity Field Recovery, Space Localizing Basis Functions, VCE

Acknowledgments

First, I would like to thank my almighty God, who helped me in all stages of this work so that it is accomplished. My gratitude goes to my Advisor, Tulu Besha (Ph.D.). I am so grateful to my teacher Andinet Ashagrie (Ph.D.) for his support to end this work and his valuable scientific discussions and guidance during the work of this thesis.

I would like to greatly appreciate the effort and thank the Institute of Geodesy at the Graz University of Technology (ifG) for making the kinematic orbits, modeled non-gravitational forces, and background forces that I used during this study freely available. Likewise many thanks to the National Aeronautics and Space Administration (NASA) and German Aerospace Center (DLR) for making GRACE data freely available.

Contents

List of Figures

List of Tables

Abbreviations and Acronyms

ACC – Accelerometer

AF – Accelerometer Frame

CHAMP - Challenging Minisatellite Payload

CSR - Center of Space Research

CoM – Center of Mass

DEOS - Department of Earth Observation and Space Systems, TU Delft

DLR - Deutsches Zentrum für Luft- und Raumfahrt

EGM - Earth Gravitational Model

EIGEN - European Improved Gravity Model of the Earth by New Techniques

ESA - European Space Agency

FFT - Fast Fourier Techniques

GFZ - GeoForschungsZentrum Potsdam

GGM - Global Gravity field Model

GOCE - Gravity Field and Steady-State Ocean Circulation Explorer

GPS - Global Positioning System

GRACE - Gravity Recovery And Climate Experiment

GROOPS - Gravity Field Object Oriented Programming System

ICRF - International Celestial Reference Frame

IPU – Internal Processing Unit

IERS - International Earth Rotation and Reference Systems Service

ITG - Institut fuer Theoretische Geodäsie, Universität Bonn

ITRF - International Terrestrial Reference Frame

JPL - Jet Propulsion Laboratory

KBR - K-Band Ranging System

LEO - Low Earth Orbiter

LOS - Line of Sight

MER - Main Ethiopian Rift

NASA - National Aeronautics and Space Administration

POD - Precise Orbit Determination

RKHS - Reproducing Kernel Hilbert Space

RMS - Root Mean Square (Error)

SCA – Star Camera

SOE – Sequence of Events File

SDS - Science Data System

SLR - Satellite Laser Ranging

SRF - Science Reference Frame

SST - Satellite-to-Satellite tracking

SGG – Sequence of Events File

TOF – Time of Flight

USO – Ultra Stable Oscillator

VCE - Variance Component Estimation

UTCSR - University of Texas in Austin, Center for Space Research

XML - Extensible Markup Language

Chapter One

Introduction

1.1 Background

The Earth's gravitational field gives a wealth of information about the planet as a complex dynamic system. Its accurate information is needed for geodetic and geophysical applications alike. One noteworthy example of geodetic features is the use of the geoid (i.e., an equipotential surface of the Earth's gravitational field that coincides with the mean surface of the oceans) as a reference surface for height system formulation. It is critical to know the precise position of the geoid to create a consistent global height datum. The geoid is important in calculating ocean dynamics because it represents the hypothetical ocean surface at rest. More examples of the gravity field determination importance on numerous geoscientific fields, including hydrology, glaciology, and solid Earth dynamics, can be found in the form of useful contributions. The time variable portion of the gravitational field, in particular, provides crucial insights into mass transport and variation processes (Ilk et al., 2005).

Over the last few decades, satellite data has been used to estimate the Earth's gravitational field. However, a new era has begun with the launch of new dedicated gravity field missions. The first dedicated gravity satellite mission, CHAMP (**CHA**llenging **M**inisatellite **P**ayload), had been in orbit for the period 2000 to 2010 and provided a new level of gravity field precision as well as crucial expertise for future missions. The GRACE (**G**ravity **R**ecovery **A**nd **C**limate **E**xperiment), is the second dedicated gravity satellite mission that launched in 2002. The GRACE is focused on detecting time-varying gravity field characteristics as well as identifying the static portion of the gravity field at low and medium wavelengths (Tapley et al., 2005).

For the first time, temporal and spatial fluctuations in continental water storage have become apparent on a worldwide scale due to GRACE data. The third dedicated gravity satellite mission is GOCE (**G**ravity Field and Steady-State **O**cean **C**irculation **E**xplorer), which launched in 2008. Its goal was to retrieve the high-resolution static component of the gravitational field with high precision. The observations' in-situ character is a novel concept for the new gravity field missions.

Continuous observation of each satellite's orbit is feasible since each satellite is equipped with a GPS receiver. Furthermore, the extra data (precise inter-satellite ranges and range rates in the case of GRACE, and gradiometer readings in the case of GOCE) enables the use of the gravitational field more or less directly, emphasizing the in-situ nature(Eicker, 2008).

The novel observation types do not need a long-term investigation of satellite orbits and can deal with short arcs of the satellite's orbit, unlike prior attempts to derive gravity fields from satellite data. This is a critical characteristic that enables regional gravity field solutions to be calculated using satellite data gathered over a defined geographic region. Despite the outstanding findings gained so far by the satellite missions, it is expected that the data can yield much more information.

In this setting, regional modeling is one possibility. The gravity field modeling based on a spherical harmonic expansion does not adequately describe regional gravity field peculiarities. The signal content of the gravitational field varies significantly between geographic regions. In particular, in the higher frequency ranges of the spectrum. Global support basis functions, such as spherical harmonics, are unable to adequately account for these geographical differences. The degree of instability in the gravity field recovery process varies by region and increases with increasing frequencies in the gravity field signal. When a global regularization is used to account for the ill-posedness of the downward continuation process, the data are filtered globally, resulting in a mean dampening of the global gravity field features. As a result, a locally tailored regularization strategy is expected to retrieve more information from a given signal than a global analysis would.

The generation of regional gravity field models using satellite data may be done in several ways. A variety of distinct gravity field representations employing space localizing basis functions were developed to parametrize the gravity field solutions. Regional approaches can also be used to combine globally distributed satellite data with small-area terrestrial data sets.

1.2 Statements of the Problems

So far, the most common method of characterizing the Earth's gravitational field has been to expand in terms of spherical harmonics. Despite the good findings so far, it is likely that the signal content in satellite observations hasn't been used to its full potential. There are a number of causes for this, but one key factor is poor background force modeling (such as ocean tides or atmospheric variations), which is thought to be the primary reason behind it.

Inadequate modeling of satellite data employing spherical harmonics in a global form might also contribute to sub-optimal signal exploitation. It is reasonable to tailor the analysis technique to the individual features of the gravitational signal found in different regions to fully recover the signal information included in satellite and sensor data. The parameters of the gravitational field vary substantially between geographical locations, particularly in the higher frequency region of the spectrum.

These heterogeneities are caused by different topographical characteristics with rough gravity signals, such as those formed by mountain areas or deep-sea tunnels, and smooth signal areas, such as those seen in parts of the open ocean. This analysis method is designed to densely observed short arcs of the satellite's orbit and considers the in-situ character of the observations, has enabled regionally restricted satellite data to be utilized to analyze the gravitational field in the appropriate geographical places. The technique used in this study is based on a global reference model represented by spherical harmonics, and it involves calculating regional refinement in the study area. Radial basis functions with local (or nearly local) support should be used to model these regional solutions. The resolution of the parameterization can be modified in this method based on the gravity field signal in the region. However, not only should the parameterization be tuned to each location's unique characteristics, but the entire analysis technique should be modified to provide the best regionally tailored findings. In this context, it is important to emphasize the regularization process that is required in connection with the downward continuation process, (e.g Eicker et al., 2004; Ilk et al., 2007; Eicker et al., 2006).

The dedicated gravity satellite mission observations are filtered overall by a uniform global regularization parameter, resulting in a mean dampening of the global gravity field features. Then there is the issue of extra information in the gravity signal being muted unnecessarily much in parts with rough gravity field characteristics. But in regions with a smooth gravity signal, a stronger regularization is recommended. This method allows for the extraction of more information from the given data than is possible with global gravity field determination.

Ethiopia is known for its complicated topographic and geological features. Extreme undulation characterizes the topography. Only Eshagh et al., (2018) used GOCE gradiometer data to recover the gravity anomaly in Ethiopia. Because of this, in the study area of this research (i.e Ethiopia), the regional refinement procedure is required for the extraction of more information using GRACE data over the area.

1.3 Objectives

1.3.1 General Objectives

The main objective of this study is to determine the regional gravity field as a refinement to the global model, using Radial Basis Functions over Ethiopia.

1.3.2 Specific Objectives

The specific objectives of the research were

- To calibrate the raw ACC1B accelerometer data using modeled non-gravitational data
- To identify optimal radial basis distribution over the study area
- To evaluate the capability of the regional refinement method to be employed, for the regional gravity field recovery over the study area

1.4 Significance of the Study

The significance of the research is primarily in contributing to the reduction of noise in smooth gravity field features and the extraction of additional signals in higher frequency areas within the study area.

1.5 Organization of the Thesis

The thesis is organized around six chapters: the first chapter introduces the basic concept of Regional gravity field refinement and its importance in extracting signals which are not included due to the nature of the global model basis functions, and spherical harmonics. Also states the objectives of the study, describes the statement of the problem, the limitation of the study as well as the overview of the study area.

Chapter two discusses literature reviews related to this study, fundamentals of physical geodesy, space localized basis functions, point distribution on the sphere, and existing and new regional gravity techniques in general. Chapter three focuses on data sources and methodology rationale. The details of the data source, the working principles, geometry of satellites configuration, a mathematical model for observation equations, and methods for solving the required unknown parameters. Data resampling, data screening, and accelerometer calibration methods are described. Chapter four explain the data analysis and processing of the accelerometer, parameterization of RBFs in detail, and analysis of the outputs. Chapter five presents the result and discussion of the thesis. Lastly, chapter six covers the topics of conclusion and recommendation.

1.6 Overview of the Study Area

Ethiopia is the study area, with latitudes ranging from 3° N to 15° N and longitudes ranging from 33° E to 48° E. This area is further extended by 10° to reduce the effect of the STE of the integral formula. As a result, the data and recovered data will have a boundary between -7° N and 25° N latitudes and 23° E and 58° E longitudes. Ethiopia is known for its complicated geographical and geological features.

The Main Ethiopian Rift (MER) divides the country's landmass into two plateaus: eastern and western. Between the Nubia and Somalia plates is the Main Ethiopian Rift (MER). It stretches from the Afar triple junction in northern Kenya to the Lake Turkana valley (Wolfenden et al., 2004; Keir et al., 2009).

In the MER's southern, middle, and northern portions, there are numerous active volcanoes. The Afar triangle is a geologically active area on our planet, where three plates converge: the Nubia-Somalia, Arabia, and Africa plates.

Many geophysical investigations have been carried out to better understand the rifting process' geodynamics (Furman et al., 2006). In terms of volcanism, seismicity, and tectonic deformation, many recent studies have indicated that the MER is quite active (Ebinger et al., 2010; Bastow et al., 2008).

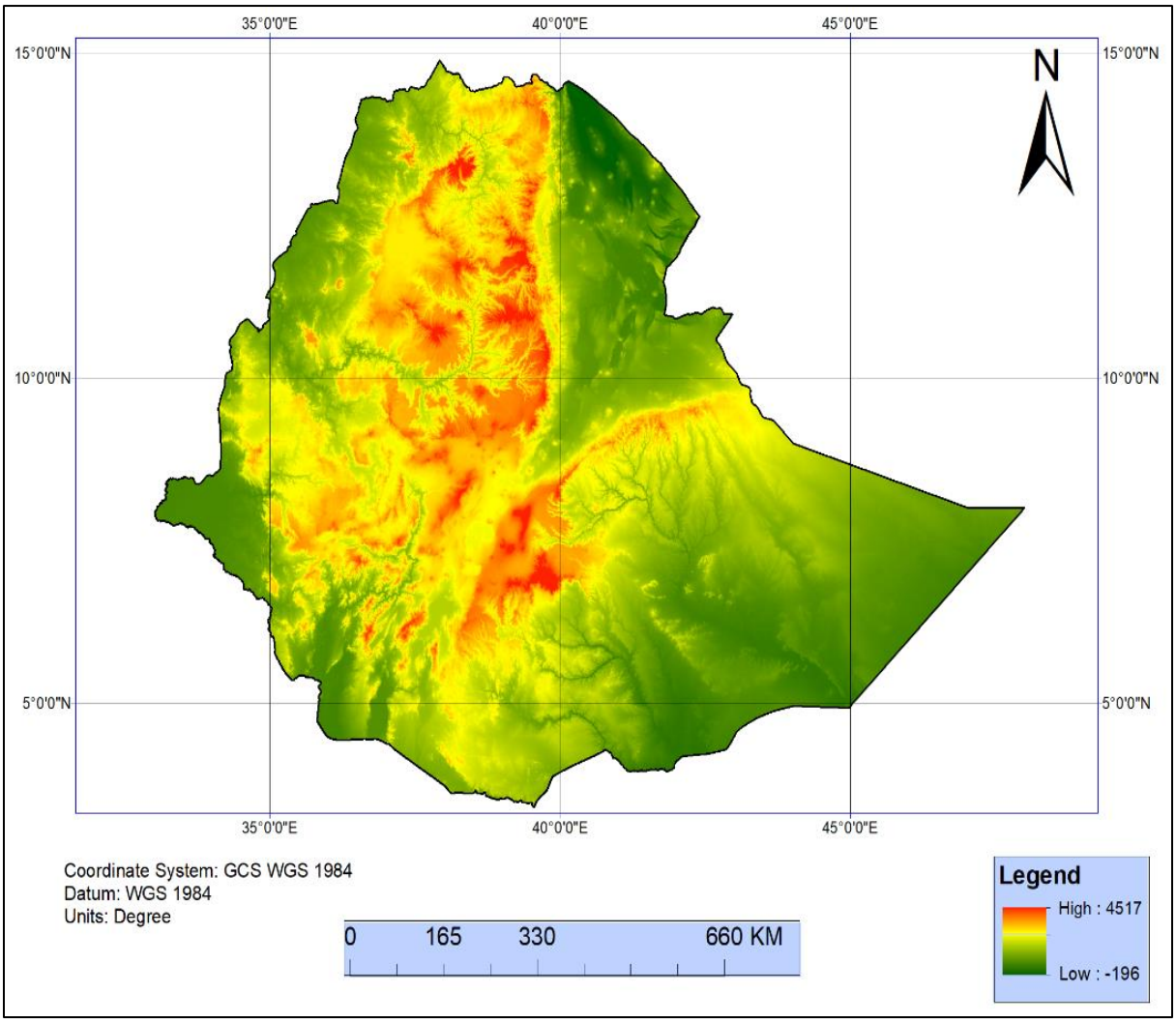

Figure 1.1 Study area and its topographic regime [meters]

Chapter Two

Literature Review

2.1 General Overview

The existing gravity field models obtained from GRACE mission data (Tapley and Reigber, 2001) have given us remarkable precision in gravity field determination. Despite this, the predicted GRACE baseline accuracy has yet to be met. One problem, among many, might be inadequate modeling of satellite data using a global representation by spherical harmonics. It appears appropriate to enhance global solutions by regional recovery procedures to extract the signal information included in satellite and sensor data to full content. Varied geographical places have different gravity field characteristics, especially in the higher frequency section of the spectrum. As a result, the recovery procedure should be tailored to the specific features of the region.

2.2 Fundamentals of Physical Geodesy

The principles of physical geodesy are covered in this section. Heiskanen and Helmut Moritz are notable pioneers in the subject of physical geodesy, and the resources given below are based on their book, i.e. Heiskanen and Moritz (1967).

2.2.1 Newton's Gravitational Law

This section gives a quick overview of potential theory. The force of attraction between two bodies of mass m_1 and mass $m_2$at a distance *r* from one other is provided by Newton's law of gravity as,

$$F = G\frac{m_1 m_2}{r^2}, \tag{2.1}$$

where $G = (6.6742 \pm 0.0010) \cdot 10^{-11} m^3/kg\ s^2$ is newton's gravitational constant. The combination of Eq. (2.1) with Newton's second law $F = ma$, this in the situation of constant masses, gives the acceleration of the body of mass m_1 with respect to the center mass of both bodies as,

$$a = \frac{Gm_2}{r^2}. \tag{2.2}$$

The equivalence principle allows a vector representation of the acceleration $\boldsymbol{a}$ or $\boldsymbol{g}$ to be obtained by deriving the acceleration from a scalar function called gravitational potential(V). The Laplace equation is true for the Earth's exterior, and the gravitational potential may be represented using spherical harmonic functions. This is essential because it establishes the foundation for the construction of different potentials in terms of spherical harmonics.

2.2.2 Important Relations in Physical Geodesy

Forces or accelerations acting on an arbitrary body on the surface of the Earth must first be specified. The gravitational acceleration, $\boldsymbol{g}_{grav}$, which is generated by the gravitational attraction of Earth's mass, and the centrifugal acceleration $\boldsymbol{g}_{cen}$, which is caused by Earth's rotation, are the two major accelerations. The latter is proportional to the distance from the Earth's rotation axis and reaches its maximum near the equator, while it vanishes at the poles. These forces also influence a gravimeter that is located on Earth. Additionally, solar system masses (such as the sun and moon) must be included since their motion relative to the Earth introduces a time-varying field. Potentials are generated by all masses in potential theory. The gravitational potential V exists on the one hand, and the centrifugal potential Φ exists on the other, both of which cause accelerations. The combination of gravitational and centrifugal acceleration is indicated as gravity vector $\boldsymbol{g}$ in the first step, and it follows,

$$\boldsymbol{g} = \boldsymbol{g}_{grav} + \boldsymbol{g}_{cen} \tag{2.3}$$

where every single acceleration is equipped with an associated potential. The gravitational potential of the Earth is then calculated using

$$W = V + \Phi. \tag{2.4}$$

Generally, the potential is defined as the amount of work required to move a mass from one point to infinity (Heiskanen and Moritz, 1967). If such an equipotential surface corresponds with the mean sea surface, it is referred to as a geoid. For height systems, it serves as a reference surface. The gradient operator on the Earth's gravitational potential W may be used to represent the gravity vector ($\boldsymbol{g}$).

$$g = \nabla W = \left(\frac{\partial W}{\partial x}\frac{\partial W}{\partial y}\frac{\partial W}{\partial z}\right)^T \tag{2.5}$$

The scalar absolute gravity value is determined by the magnitude of the gravity acceleration vector $\|\boldsymbol{g}\|$. Gravity has the physical dimension of acceleration and is measured in gal, called after Galileo Galilei. With, a link to SI units is provided.

$$1\ gal = 0.01\ {}^{m}/_{s^2} \tag{2.6}$$

The same relation also holds for the gravitational potential, where the derivatives are related to the components of the gravitational acceleration according to

$$\boldsymbol{g}_{grav} = \nabla V = \left(\frac{\partial V}{\partial x}\frac{\partial V}{\partial y}\frac{\partial V}{\partial z}\right)^T \tag{2.7}$$

This also holds for the centrifugal potential. For several point masses, the superposition principle is valid,

$$V = \frac{Gm_1}{l_1} + \frac{Gm_2}{l_2} + \cdots + \frac{Gm_n}{l_n} = G\sum_{i=1}^{n}\frac{m_i}{l_i} \tag{2.8}$$

where G is the gravitational constant and m_i the mass of the attracting point. The Euclidean distances are denoted with l_i. Assuming a continuous mass distribution and a corresponding density ρ, the gravitational potential can be expressed as Newtonian volume integral formula according to,

$$V = G\iiint_{\Omega}\frac{\rho}{l}\,d\Omega \tag{2.9}$$

Furthermore, a point that is located outside the masses fulfills the Laplace equation which is characterized as harmonic.

$$\Delta V = \frac{\partial^2 V}{\partial x^2} + \frac{\partial^2 V}{\partial y^2} + \frac{\partial^2 V}{\partial z^2} = 0 \tag{2.10}$$

This in turn provides the opportunity to represent the exterior potential by spherical harmonics. For the interior potential, the Poisson equation is valid because of the non-vanishing density according to

$$\Delta V = -4\pi G\rho \tag{2.11}$$

2.2.3 Spherical Harmonics

The gravitational potential V may be expanded into spherical harmonics since the external potential is described as harmonic. To solve the Laplace equation Eq. (2.10), one option is to represent it in spherical coordinates. The Laplace equation is a second-order partial differential equation that is written as follows in spherical coordinates:

$$r^2\frac{\partial^2 V}{\partial r^2} + 2r\frac{\partial V}{\partial r} + \frac{\partial^2 V}{\partial \vartheta^2} + cot\vartheta\frac{\partial V}{\partial \vartheta} + \frac{1}{sin^2\vartheta}\frac{\partial^2 V}{\partial \lambda^2} = 0 \tag{2.12}$$

Two possible solutions of this differential equation are given for the interior $[i]$ and the exterior $[e]$ potential of a unit sphere as

$$V^i(r,\vartheta,\lambda) = \sum_{n=0}^{\infty} r^n Y_n(\vartheta,\lambda), \tag{2.13}$$

$$V^e(r,\vartheta,\lambda) = \sum_{n=0}^{\infty} \frac{1}{r^{n+1}} Y_n(\vartheta,\lambda), \tag{2.14}$$

with $Y_n(\vartheta,\lambda)$ as the Legendre surface spherical harmonics, which in turn can be reformulated to the following equations, either

$$Y_n(\vartheta,\lambda) = P_{nm}(cos\vartheta)cosm\lambda, \tag{2.15}$$

$$Y_n(\vartheta,\lambda) = P_{nm}(cos\vartheta)sinm\lambda, \tag{2.16}$$

where the P_{nm} are the associated Legendre functions and n and m denote the degree and order. The Legendre functions can be found according to

$$P_{nm}(t) = (1-t^2)^{\frac{m}{2}}\frac{d^m P_n(t)}{dt^m} \quad \text{with} \quad P_n(t) = \frac{1}{2^n n!}\frac{d^n}{dt^n}(t^2-1)^n \quad and \quad t = cos\vartheta \tag{2.17}$$

After a combination of all possible solutions to the differential equation, the Laplace series reads

$$Y_n(\vartheta,\lambda) = \sum_{n=0}^{\infty}[c_{nm}P_{nm}(cos\vartheta)cosm\lambda + s_{nm}P_{nm}(cos\vartheta)sinm\lambda] \tag{2.18}$$

where the c_{nm} and s_{nm} are coefficients.

2.2.4 Potential and Linearization

Some approximations of the Earth's gravity field are required to connect the non-linear relation of gravity field observables with unknown ones. An approximation must ensure only minor deviations from the actual gravity field to consider a linear relationship between these quantities. As a result, as an appropriate counterpart of the Earth, an ellipsoid of revolution with a matching normal potential is introduced, which is briefly discussed in the following.

Normal Potential

The idea behind the normal potential representation is to divide the Earth's gravity potential W into two parts. One normal part, with normal gravity and normal potential, and a small supplement, both of which are related to a rotating ellipsoidal reference surface. A rotating ellipsoid may thus be chosen to assure a resemblance to the Earth's form, with the benefit of being able to carry out the computation in a rigorous mathematical manner. A proper approximation of Earth's geometry and gravity is necessary for physical geodesy to perform a linearization between geodetic observables and the Earth's gravity field, which is in general a nonlinear relationship. As a result, a rotationally symmetric ellipsoid is employed, with a global deviation of less than $\pm$ 100 m from the actual geoid. According to (Heiskanen and Moritz, 1967), the normal potential can be written as,

$$U = V_{ell} + \Phi \tag{2.19}$$

where V_{ell} is the ellipsoid's gravitational potential and Φ is the centrifugal potential. The closed formulae that describe the normal or ellipsoidal potential may be found in, for example (Moritz, 1980ba). The Somiglianas formula is used to calculate the normal gravity magnitude.

$$\gamma_0 = \frac{a\gamma_e cos^2\varphi + b\gamma_p sin^2\varphi}{\sqrt{a^2cos^2\varphi + b^2sin^2\varphi}}, \tag{2.20}$$

where γ_e and γ_p denote the gravity at the equator and poles, respectively. The ellipsoid's major and semi-major axes are represented by the letters a and b. Normal gravity is just a function of the geodetic latitude because of the ellipsoid's rotational symmetry. Somiglianas formula is only valid on the ellipsoidal surface. The gravity in an arbitrary ellipsoidal height h can be approximated by a truncated series expansion according to

$$\gamma(h) = \gamma_0 \left[1 - \frac{2}{a}(1 + f + m - 2f sin^2\varphi)h + \frac{3}{a^2}h^2\right], \tag{2.21}$$

with the ellipsoidal flattening,

$$f = \frac{a - b}{a} \tag{2.22}$$

The quality of the geoid approximation is determined by the reference ellipsoid selected. According to (Moritz, 1980b), a common approach is to utilize the GRS80 ellipsoid as a reference field. The gradient operator applied to the appropriate potential $\gamma = \nabla U$ can be used to determine the normal gravity vector in general.

Centrifugal Potential

The centrifugal potential Φ is a component of the relationship between the gravity potential W and the normal potential U of the Earth. The following is a simple analytical representation in Cartesian coordinates:

$$\Phi = \frac{1}{2}\omega^2(x^2 + y^2) \tag{2.23}$$

where ω represents the Earth's rotational angular velocity. The components of the centrifugal potential may be determined using the first derivative of the potential in the same way as the gravity and normal potentials according to,

$$\nabla\Phi = \left(\frac{\partial\Phi}{\partial x} \;\; \frac{\partial\Phi}{\partial y} \;\; \frac{\partial\Phi}{\partial z}\right)^T \tag{2.24}$$

If the Laplace operator is applied to the centrifugal potential,

$$\Delta\Phi = \frac{\partial^2\Phi}{\partial x^2} + \frac{\partial^2\Phi}{\partial y^2} + \frac{\partial^2\Phi}{\partial z^2} = 2\omega^2 \tag{2.25}$$

it reveals that Φ is not harmonic. The centrifugal acceleration depends on the distance to the Earth's rotational axis and acts in the opposite direction to the gravitational acceleration. As a consequence, the centrifugal acceleration increases as one approaches the equator(Moritz, 1980a).

Disturbing Potential

Because the reference ellipsoid is simply an approximation of the geoid and the true gravity field, the relationship between the gravity potential of the Earth W and the normal potential U, which is commonly employed as a reference potential, is affected by a small difference. Disturbing potential T is the name given to the potential difference. The following relationship holds if the geoid and the reference ellipsoid are fairly similar.

$$W = U + T \tag{2.26}$$

Outside of the attracting masses, the disturbing potential fulfills the Laplace equation, thus $\Delta T = 0$ is valid. A good approximation of the actual field results in a small residual fraction, which allows for a truncated Taylor series expansion. As a result, the disturbing potential might be stated as,

$$T = W - U = V - V_{ell}. \tag{2.27}$$

It is possible to represent the series in terms of spherical harmonics, and owing to the elimination of the centrifugal potential, the series eventually reads

$$T(r, \vartheta, \lambda) = \frac{GM}{R} \sum_{n=0}^{\infty} \left(\frac{R}{r}\right)^{n+1} \sum_{m=-n}^{n} \Delta\bar{a}_{nm} \bar{Y}_{nm}(\vartheta, \lambda)\,. \tag{2.28}$$

The coefficients $\Delta\bar{a}_{nm}$ represent the linearized difference of the two fully normalized potentials in the spectral domain. The derivatives of the disturbing potential are also important and provide a connection of the individual gravity field quantity to the disturbing potential which can, in turn, be expressed in spherical harmonics.

2.2.5 Functionals of the Disturbing Potential

Gravity Anomalies

Gravity anomalies are typically defined as the difference in vectors between a point P_o on the geoid and a point Q on a reference ellipsoid, as shown in Fig. 2.1.

The appropriate normal gravity vector γ is introduced as a Taylor point for the linearization in this original definition, which is based on a normal field ellipsoid. Gravity anomalies are defined in vector notation as,

$$\Delta \boldsymbol{g} = \boldsymbol{g}_P - \gamma_Q \tag{2.29}$$

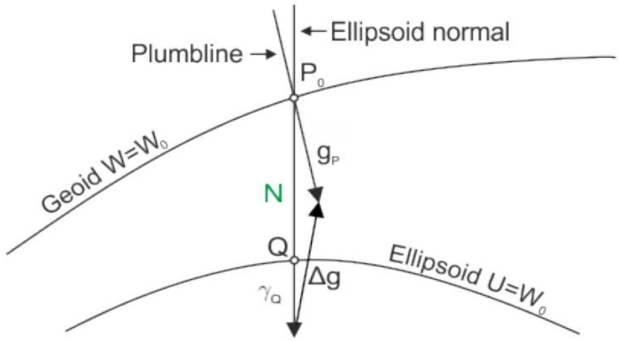

Figure 2.1: Common definition of gravity anomalies

It is also vital to understand that deflections of the vertical occur when the directions of both gravity vectors, $\boldsymbol{g}_P$, and γ_Q are evaluated at the same location on the Earth's surface. In a spherical approximation, gravity anomalies can be represented by the fundamental equation of physical geodesy.

Gravity Disturbances

A second quantity of the disturbing potential, namely the gravity disturbance, is required to obtain the fundamental equation of physical geodesy. The gravity disturbance vector was first defined by comparing the gravity vector $\boldsymbol{g}$ with the normal gravity vector γ at the same position, P.

Because vectors may be shifted in their line of action, this is easy to do. The magnitude difference between the actual and normal gravity vectors is

$$\delta \boldsymbol{g} = \nabla T = \boldsymbol{g}_P - \gamma_P \tag{2.30}$$

and generally, this corresponds to the gradient of the disturbing potential T. The scalar-valued gravity disturbance reads

$$\delta g = -\frac{\partial T}{\partial r}, \tag{2.31}$$

which gives the gravity disturbance and its connection to the disturbing potential (Hofmann-Wellenhof & Moritz, 2006). The gravitational disturbance is described in terms of spherical harmonics by the radial derivative of the disturbing potential, which is provided in Eq. (2.28).

$$T_r = \delta g = -\frac{GM}{R^2}\sum_{n=0}^{\infty}(n+1)\left(\frac{R}{r}\right)^{n+2}\sum_{m=-n}^{n}\left[\Delta\bar{c}_{nm}\cos m\lambda + \Delta\bar{s}_{nm}\sin m\lambda\right]\bar{P}_{nm}, \qquad (2.32)$$

The common definition of gravity disturbance is shown in Fig. 2.2. The radial component represents the difference in terms of magnitude.

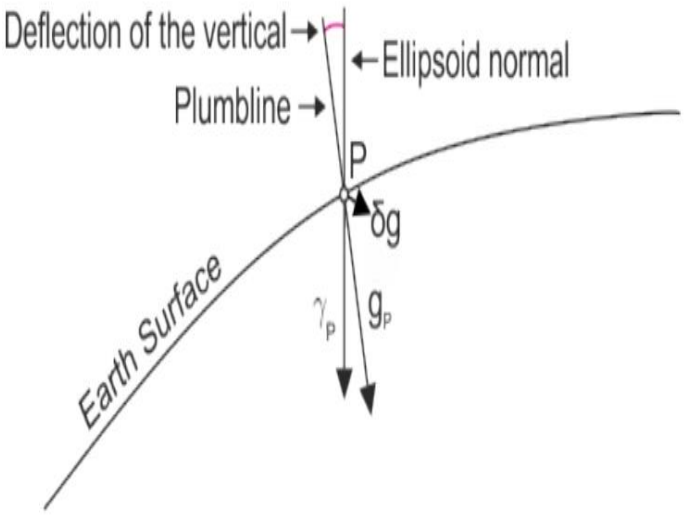

Figure 2.2: Common definition of the gravity disturbance

Geoid Heights

Bruns equation (Bruns, 1878) defines the relationship between the disturbing potential and the geoid height.

$$N = \frac{T}{\gamma} \qquad (2.33)$$

If the disturbing potential is evaluated on the geoid surface, this equation is utilized to determine the geoid.

Plugging Eq. (2.28) into Eq. (2.33), the geoid in terms of spherical harmonics may be determined by,

$$N = \frac{GM}{R\gamma} \sum_{n=0}^{\infty} \left(\frac{R}{r}\right)^{n+1} \sum_{m=-n}^{n} [\Delta\bar{c}_{nm} cos\, m\lambda + \Delta\bar{s}_{nm} sin\, m\lambda]\, \bar{P}_{nm}. \tag{2.34}$$

2.3 Space Localizing Basis Functions

A function can be localized in both the space and frequency domains. The extent of the area in the specified domain where the function does not vanish is referred to as 'localization'. The function localizes better the smaller this area is. According to Heisenberg's uncertainty principle, a function cannot exhibit perfect localizing properties in both the frequency and space domains at the same time (Heitz and Stöcker-Meier, 1994). The ratio of both localizations is reciprocally proportional because of better the function localizes in one domain, the less it localizes in the other. The corresponding localization properties are also assigned to the different basis functions in Fig. 2.3, which is a schematic figure of the issue.

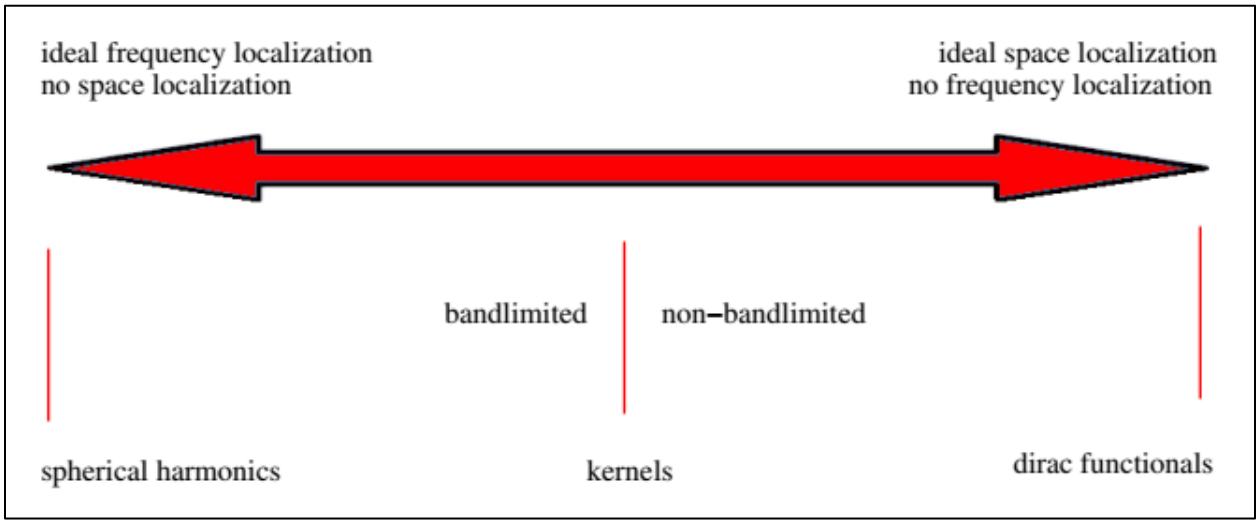

Figure 2.3: Uncertainty principle (Freeden, 1999; Eicker, 2008)

In the frequency domain, the spherical harmonics have perfect localizing characteristics, because each degree n and order m may be related to a single frequency.

As a result, in the space domain, they have no localizing properties at all (i.e each spherical harmonic is considerably different from zero all over the sphere). This is because spherical harmonics are basis functions with global support. As a result, changes in one coefficient always have an impact on the entire sphere. Changes in a geographically limited part of the represented field, on the other hand, will influence the whole set of spherical harmonic coefficients. Consequently, calculating a single field value necessitates evaluating all of the global model's coefficients. The Dirac functionals are provided by the opposite properties. They differ from zero in just one point in the space domain, resulting in complete localizing qualities in that location. They, on the other hand, give equal weight to each frequency and, as a result, show no localization in the frequency domain. Kernels, such as the ones that will serve as the basis functions for regional modeling, allow a compromise between spatial and frequency localization (Eicker, 2008).

Kernels are different from zero only in a geographically confined region or decay rapidly enough in the space domain to be regarded as quasi-space localizing, despite the fact that they do not have full localization in the space domain. Non-bandlimited kernels are distinguished from bandlimited kernels, which have zero frequencies over a particular degree. The non-bandlimited variants have better spatial localization than their bandlimited equivalents.

2.3.1 Radial Basis Functions (RBFs)

Radial basis functions are only dependent on the spherical distance between two locations on the sphere indicated by the unit vectors x and x_i. As a consequence, they might be considered

$$\Phi_i(x, x_i) = \Phi(x \cdot x_i), \tag{2.35}$$

with $x, x_i \in \Omega$. A sum of Legendre polynomials can be used to express any radial symmetric basis function.

$$\Phi_i(x, x_i) = \sum_{n=0}^{\infty} \sqrt{2n+1} \cdot k_n P_n(x \cdot x_i) = \sum_{n=0}^{\infty} \sum_{m=-n}^{n} k_n Y_{nm}(x) Y_{nm}(x_i) \tag{2.36}$$

The shape of the function is defined by the coefficients k_n. Any functional on the sphere can be expressed as a series expansion of radial basis functions using,

$$s(x) = \sum_{i}^{I} a_i \, \Phi_i(x, x_i), \tag{2.37}$$

where a_i are scaling coefficients. x stands for the evaluation point, and the x_i denotes the nodal points where the basis functions are placed on the sphere's surface. Because the gravitational potential is a harmonic function, the radial basis functions are selected as harmonic kernel functions. This implies that they can be continued harmonically in an outward direction (Eicker, 2008).

The form of radial basis functions is determined by the coefficients k_n in Eq. (2.36), with various choices for k_n resulting in different functions.

$$\Phi_i(x_r, x_i) = \sum_{n=2}^{\infty} \sigma_n P_n(x \cdot x_i) = \sum_{n=2}^{\infty} \sum_{m=-n}^{n} \frac{\sigma_n}{\sqrt{2n+1}} Y_{nm}(x) Y_{nm}(x_i) \tag{2.38}$$

This means that the coefficients k_n in Eq. 2.36 are chosen according to (Eicker, 2008)

$$k_n = \frac{\sigma_n}{\sqrt{2n+1}} \tag{2.39}$$

The coefficients of degrees zero and one are excluded. As a result, they just need to describe a space of functions in which the zeroth and first moments vanish.

2.3.2 Bandlimited Spline Functions

So far, the basis functions have been discussed in terms of infinite-dimensional spaces. The series expansion of the basis functions must, however, be limited to a maximum degree N when dealing with actual calculations. This results in the modification of Eq. (2.36),

$$\Phi_i(x, x_i) = \sum_{n=2}^{N} \sqrt{2n+1} \cdot k_n P_n(x \cdot x_i) = \sum_{n=2}^{N} \sum_{m=-n}^{n} k_n Y_{nm}(x) Y_{nm}(x_i) \tag{2.40}$$

The omission of higher frequencies corresponds to the restriction to a maximum degree. As a result, basis functions can only model a finite-dimensional space spanned by the Y_{nm} up to degree N, yielding a smoother version of the modeled function. The expected gravity field signal to be modeled by the appropriate basis functions determines the permissible upper degree for truncation of the series expansion.

The basis functions to be employed in actual regional gravity field recovery are always applied to the parameterization of residual fields, in addition to the exclusion of the high frequencies. Therefore, they are expected to model information that is not included in a specific global reference model. As a result, the basis functions must be chosen so that they exclusively represent the residual field's spectral properties.

2.3.3 Arrangement of the Basis Functions on the Sphere

The question of the shape of the basis functions is closely related to the problem of the spline kernels' placement on the sphere being important for the distance between the nodal points of neighboring basis functions. The primary goal of the radial basis functions is to distribute them as evenly as possible across the sphere's surface. The spline kernels are inserted at the grid's nodes, resulting in a spherical grid. The given grid can be created for various degrees of resolution, with the width of the basis functions being adjusted to ensure enough coverage. Smooth modeling is impossible when, for example, spline kernels with narrow support are placed too widely apart. Using a regional recovery strategy, it would be able to adjust the resolution of the gravity field based on the signal content in different regions. In different geographical areas, this would result in different spline kernels and related grids.

In this instance, the point distribution must be established separately for each area. Furthermore, the space localizing basis functions might be used to describe specific geophysical phenomena. If this is the case, the basis functions might be arranged to best reflect the peculiarities of the specific phenomenon (Eicker, 2008).

2.4 Regional Gravity Field Modelling

Regional solutions are calculated as refinements to a global gravity field. The global reference field is usually represented by spherical harmonics, but the residual gravity field is modeled by the regional solution, which is represented by space localizing splines.

2.4.1 Existing Approaches to Regional Gravity Field Modeling

When considering the currently applied approaches to the recovery of global models, the computation of regional gravity field solutions offers many advantages, as mentioned in the previous section. As a result, this approach is growing rapidly and could be considered a valuable replacement for conventional global models. While regional gravity field solutions were previously often created using terrestrial (surface) data, regional modeling approaches have proven effective in the recovery process when employing satellite data. To take advantage of the benefits of regional analysis, it needs to employ space localizing basis functions. There is a wide range of options for selecting the appropriate basis functions for parameterization (Weightman 1967).

Mascons

Another method is to use so-called mascons to depict the gravitational field. The term 'mascons' refers to a thin layer of homogenous mass that covers a certain geographic region (such as a spherical block or cap). It was first used to describe the concentration of masses discovered on the moon (Muller and Sjogren, 1968). Rowlands et al., (2005), for example, discuss the method about current applications to data from the GRACE satellite mission. It is based on the use of differential potential coefficients to show the difference in gravitational potential induced by individual mascons. The mass element's set of potential coefficients is then scaled using the mascon parameter for each of the regional areas. Spatial and temporal restrictions are employed to ensure that pairs of mascons that are close in time or space also stay close in terms of their values and avoid numerical instabilities in the solution.

Wavelets Representation

Wavelets are a commonly used concept in the modeling of potential fields. In the literature, e.g. Holschneider (1995); Freeden et al. (1998); Schmidt (2001), a broad description of the idea of wavelets may be found in Keller (2008). The breakdown of a signal into distinct frequency-dependent detail signals is represented by wavelets. As a result, a multi-resolution representation is referred to as a wavelet representation. Scaling and wavelet functions make up the basis functions, with each wavelet function reflecting the detailed signal of a specific frequency band. They are likely to have local support in both the space and time domains.

When wavelets are used for the modeling of functions on the sphere, spherical wavelets are created. Fengler et al. (2004), used the concept to analyze CHAMP data. Schmidt (2007) modeled time-variable gravity field information from GRACE data using wavelet representations. Wavelets were employed by Schmidt et al. (2007) to depict temporally changing GRACE gravity fields. They used wavelets on the spherical harmonic coefficients of existing global spherical harmonic level 2 products. The spherical harmonic solutions were decomposed into several scales in this manner.

Slepian Functions

The Slepian technique is to design functions that concentrate a signal in the temporal and frequency domains as optimally as possible, e.g. (Slepian and Pollak, 1961; Landau and Pollak, 1962). The concept behind the technique is to maximize the spatial concentration of a strongly bandlimited function because precise localization in the time and frequency domains are mutually incompatible. The ratio of the bandlimited function's norm within the concentration region to the respective function's norm on the entire sphere may be maximized to find this function.

Baur and Sneeuw (2006) used the notion of Slepian functions in the context of analyzing data from new satellite missions, with a particular focus on the polar gap problem that arises in the case of the GOCE mission. Except for the polar gap areas, the concentration region is a spherical band. The Slepian functions have also been used to examine regional phenomena using GRACE data (Han and Simons, 2008).

2.4.2 Analysis Techniques for the New Satellite Missions

For many years, satellite data have been used to reconstruct gravity fields. The conventional method, the idea of obtaining gravity field parameters from the study of cumulative orbit perturbations of artificial satellites with varied orbit altitudes and inclinations formed the basis of the conventional method of satellite geodesy. A spherical harmonic expansion was used to represent the gravitational field because of the technique's global features. Because Satellite locations had to be calculated using discrete measurements taken from the surface of the Earth, such as accurate laser range observations, in the past due to the lack of onboard positioning systems like a GPS receiver. The differential orbit improvement technique is the name for this method. Integrating the variational equations yields the partial derivatives of the data with respect to the unknown parameters starting with initial values for the satellite's orbit.

The coverage of observations is unavoidably limited when working with topocentric observations from a small number of observation sites. To guarantee sufficient redundancy, the use of relatively long arcs spanning days or even weeks was necessary. Longer arcs were also needed to cover the periodic and secular disturbances caused by the small corrections to the estimated force function parameters. Furthermore, past gravity field missions were less sensitive to the gravity field signal and had very limited coverage due to the inclinations of the satellites' orbits because of their high orbits of more than 800 km.

The situation has fundamentally changed since the introduction of recent satellite missions (i.e GRACE, GRACE-FO, GOCE, CHAMP). A noteworthy aspect of modern missions is the nearly constant, precise observation of various satellite orbits. GRACE provides additional, very accurate K-band range and range-rate data, and the gradiometer onboard the GOCE satellite enables continuous gravity gradient observations. The gravitational field may be measured more or less directly using these measurement principles. As a result, the new observation techniques can be viewed as more in-situ measurements than analyzing cumulative orbit perturbations of artificial satellites caused by the inhomogeneous structure of the gravitational field.

Based on its basic properties, satellite-to-satellite tracking in the high-low mode, with its densely sampled data, could be understood as a more in-situ observation type than conventional observation approaches. These new in-situ observation concepts can be used in the creation of new analysis strategies. To the various sorts of observations, a range of alternative methodologies has been developed and used. The in-situ measuring principles are divided into three stages of analysis by Ilk et al. (2008).

Integral Equation of Fredholm Type

The first is based on directly relating observable, precisely defined kinematic positions to the specified force function through a Fredholm type integral equation. Mayer-Gürr et al. (2005) utilized this kind of equation to determine the CHAMP gravity models (i.e ITG Champ01e, 01k, and 01s) and Mayer-Gürr et al. (2006) applied it to GRACE data processing.

Classical Theoretical Mechanics

Both the numerical differentiation of the time series of positions and the integration of the force function are required at the second analytical level.

This capability enables the use of classical theoretical mechanics balancing equations. The energy balancing concept, in the form of the so-called Jacobi integral, has been used to calculate the CHAMP gravity field TUM-1S; for example, (Gerlach et al., 2003) was used this method to create the CHAMP gravity field TUM-1S. Other examples of the energy balancing method's application may be found in (Howe et al., 2003; Kusche and Loon, 2005; Gerlach et al., 2003). The applicability of additional energy and motion integrals in gravity field recovery and validation was studied by (Löcher and Ilk, 2005; Löcher and Ilk, 2007). Integrals derived from Newton's equation of motion three scalar components, as well as integrals based on linear and angular momentum, are among them. According to their research, alternative integrals of motion have several mathematical properties that are superior to the original Jacobi integral.

Newton's Equation of Motion

The third analytical level directly applies Newton's equation of motion, requiring the satellite positions time series to be twice differentiated. An interpolation polynomial is used to estimate the satellite positions, and the local acceleration vector is derived from the relative GPS position time series using a twice numerical differentiation of the polynomial, according to Grafarend et al. (2000); Reubelt et al. (2003); Reubelt et al. (2006); Ditmar et al. (2006), used a similar approach to determine the gravity model DEOS CHAMP-01C, utilizing weighted averages of three successive satellite locations.

Those analytical ideas adapted to the processing of in-situ observations have one thing in common: they can handle short arcs in the satellite's orbit. Splitting the orbit into smaller pieces has the benefit of keeping the cumulative impact of (residual) disturbing forces to a minimum. Furthermore, by starting a new arc after each data gap, discontinuities and gaps in the observation series may be readily addressed. Furthermore, the use of small arcs allows for the calculation of the gravitational field in a given location using satellite measurements originating from arcs encompassing the area. For the computation of regional gravity field solutions, this is an unavoidable need. As a result of the improved observation and analysis processes, regional gravity field analysis as a way of refining global solutions is now possible.

Conventional analytical methodologies based on the integration of variational equations, on the other hand, are still being implemented to great effect on new satellite missions.

2.5 Regional Gravity Field Recovery in Ethiopia

Ethiopia is known for its complicated topographic and geological features. Extremely undulating topography characterizes the topography. The Main Ethiopian Rift divides the country's landmass into two plateaus: eastern and western. Between the Nubia and Somalia plates is the Main Ethiopian Rift (MER). It ranges from the Afar triple junction in northern Kenya to the Lake Turkana valley (Wolfenden et al., 2004; Keir et al., 2009). Most of the studies related to gravity conducted in Ethiopia are specific to understanding the rifting process. The main target of these studies was the Afar triangle which is an area of active extensional tectonics and basaltic magmatism from which the Gulf of Aden, the red sea, and the Ethiopian rift system radiate. The use of space-borne data to study gravity in Ethiopia is not well implemented.

Only the GOCE mission was used to recover a gravity anomaly in Ethiopia with a resolution of $1°x1°$ at sea level utilizing diagonal components of the gravitational tensor(Eshagh et al., 2018). The anomaly errors are computed, and recovery from these diagonal components is examined for their relevance. When compared to their errors, the difference between the recovered anomalies from each scenario is statistically insignificant. They were able to enhance the result by around 1 $mGal$ by inverting the diagonal components jointly.

2.6 GRACE Satellite Mission and Data

GRACE Level-1B RL02 data products, which include inter-satellite range rates derived from the K-Band link between the two satellites, attitude data from the star cameras, non-gravitational accelerations measured by the accelerometer, and orbit information, are used to refine the global model regionally. In addition to the official Level-1B, the input data includes kinematic orbits computed at the IfG (Zehentner and Mayer-Gürr, 2016). The Level-1B data items are pre-processed before the actual gravity field recovery. This yields a calibrated accelerometer data product, which can be used instead of the official accelerometer data product (ACC1B) in subsequent modeling. The RL03 official data product yields an improved attitude data product.

2.6.1 Overview of the Mission

GRACE is a joint scientific satellite mission between the National Aeronautics and Space Administration (NASA) in the United States and the German Aerospace Center (DLR). In 1996, it was presented by the University of Texas at Austin's Center for Space Research (CSR), the German Research Centre for Geosciences (GFZ), NASA's Jet Propulsion Laboratory (JPL), Space Systems/Loral (SSL), the DLR, and Astrium GmbH, and the second mission in the series was approved by NASA's Earth System Science Pathfinder (ESSP) program in 1997 (Tapley et al., 2005). The GRACE mission consists of two identical satellites, GRACE-A and GRACE-B, following each other in the same orbital track, linked by a highly accurate inter-satellite K-Band microwave ranging system. Fig. 2.4 depicts the satellite constellation. On March 17, 2002, GRACE was successfully launched from the Russian spaceport of Plesetsk aboard a Rockot launch vehicle.

With an initial height of about 500 km and a notional along-track separation of 220 km, the twin satellites were placed in a near-circular and near-polar orbit. The orbit has naturally declined since then, reaching an altitude of around 320 kilometers at the end of the science mission. GRACE stopped science operations in October 2017 after more than 15 years of service owing to an age-related battery issue on GRACE-B. GRACE-B re-entered the Earth's atmosphere on December 24, 2017, and burned up.

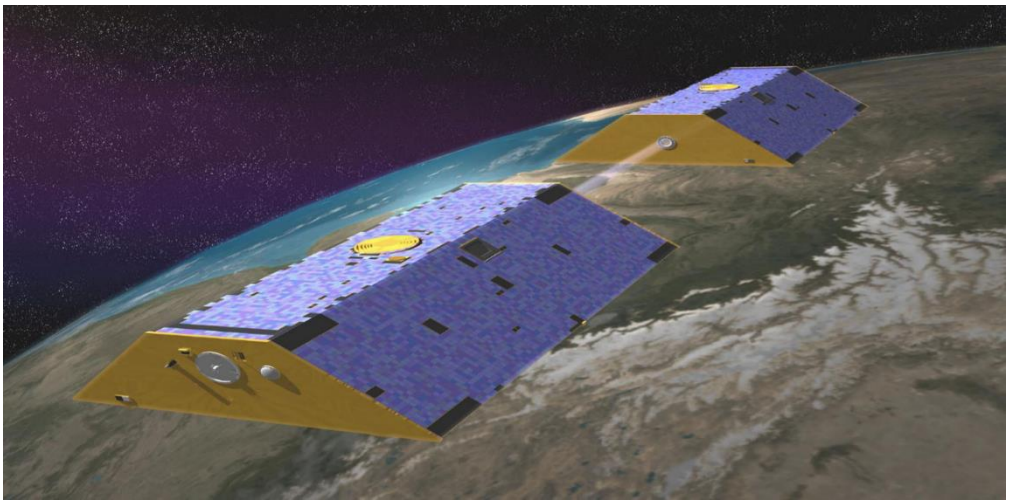

Figure 2.4: Illustration of the GRACE twin satellites in orbit. Source: NASA/JPL

2.6.2 Scientific Goals

The GRACE mission's major scientific goal is to obtain accurate global models for the mean and time-variable components of the Earth's gravitational field (Stanton et al., 1998). Each satellite has a science payload that includes a K-Band microwave ranging (KBR) system that measures the inter-satellite distance with micrometer accuracy, a Global Positioning System (GPS) receiver for position determination and radio occultation measurements, star cameras (SCA) for precise attitude determination, and an accelerometer (ACC) that measures the non-gravitational forces acting on the satellite.

GRACE was the most successful gravity field mission so far, providing information on the Earth's static and time-variable gravity field for more than 15 years. Because the gravity field is an important indicator of mass variations within the dynamic system Earth, the observation of mass changes from time-variable gravity has become a major topic among scientists, particularly in global climate research. The precise knowledge of the gravity field and its variations is a unique and invaluable source of data for a variety of environmental and geophysical research areas, allowing fundamental insights into the global water cycle, polar and mountain ice mass loss, changes in ocean surface currents, sea-level rise, groundwater depletion, and many other processes.

2.6.3 Mission Design - Measurement Principle

GRACE is based on the Satellite-to-Satellite Tracking (SST) measurement principle, which uses satellites to track other satellites (cf. Fig. 2.5). In general, there are two types of SST:

High-low Satellite-to-Satellite Tracking (hl-SST):

Several high-altitude satellites with precisely defined orbits, such as GNSS (Global Navigation Satellite System) satellites, are used to determine the orbit of a Low Earth Orbit (LEO) satellite.

Low-low Satellite-to-Satellite Tracking:

Two satellites are in the same orbit, separated by only a few hundred kilometers. Changes in the relative distance between the two satellites are caused by irregularities in the Earth's gravity field, which can be monitored by an onboard ranging device.

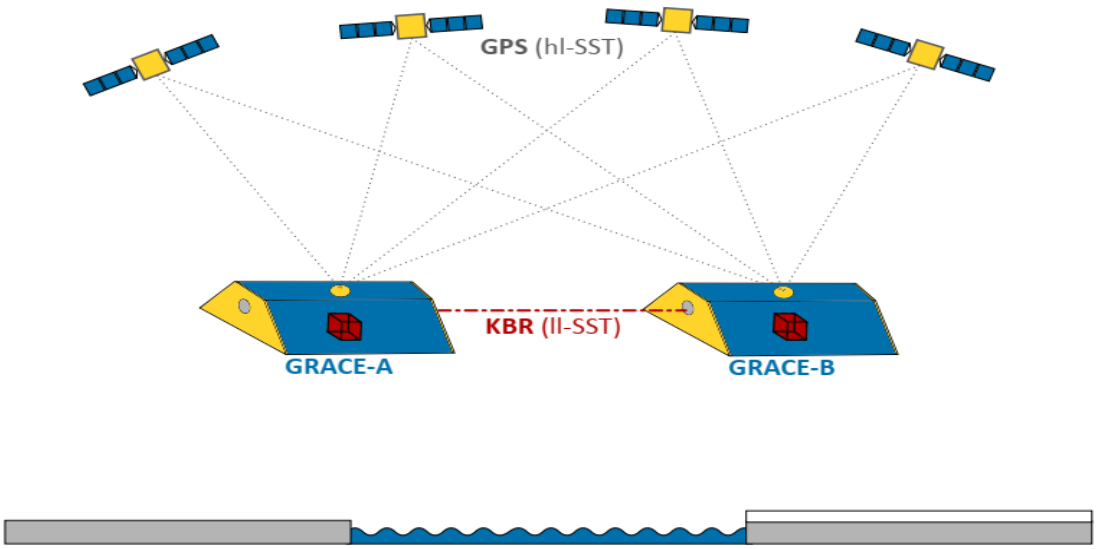

Figure 2.5: GRACE measurement principle: hl-SST and ll-SST source(Kvas et al., 2019)

GRACE, a dual-satellite mission, uses both techniques to calculate the Earth's gravitational field, using (1) continuous GPS orbit tracking data (hl-SST) and (2) inter-satellite tracking data (ll-SST: ranges, range-rates, range-accelerations) measured by the onboard KBR system.

The two GRACE satellites (GRACE-A and GRACE-B) are in a near-circular (e = 0.005) and near-polar $I = 89°$ orbit. This orbital arrangement ensures that any normal 30-day span, which is the nominal interval for GRACE monthly gravity field solutions, has sufficient spatial coverage. Throughout the mission, the orbit height decreases from almost 500 kilometers at the start to around 300 kilometers at the end. Aside from altitude loss, the orbital plane's orientation relative to the Sun (angle) changes every 322 days.

Both GRACE satellites experience gravitational perturbations while they orbit the Earth due to inhomogeneous mass distribution and re-distribution (e.g., mass exchange between land, ocean, and atmosphere) within the system Earth. Because the two spacecraft are separated by 170 km to 270 km in a co-planar orbit, the leading and trailing satellites detect slightly different disturbances, resulting in constant inter-satellite distance fluctuations. The GRACE KBR system measures these range changes very precisely.

Non-gravitational effects like an atmospheric drag, solar radiation pressure, and albedo cause perturbations to the satellites in addition to gravitational disturbances. As a result, the GRACE satellites are equipped with highly sensitive accelerometers that measure the non-gravitational accelerations acting on the spacecraft directly. This assures that the non-gravitational accelerations differential range changes are appropriately removed (from the GRACE inter-satellite tracking measurements).

The recovery of highly precise temporal gravity field models is possible using a combination of GPS hl-SST, KBR ll-SST, and accelerometer. In comparison to other gravity field missions like CHAMP or GOCE, differential KBR measurements increase the long and medium wavelengths and allow for the observation of temporal fluctuations in the Earth's gravity field.

K-Band Inter-Satellite Ranging

The KBR Assembly is the GRACE mission's principal science instrument, giving dual one-way range measurements with micrometer-level accuracy. It uses phase tracking of K-band (24 GHz) and Ka-band (32 GHz) signals sent between the two GRACE spacecraft to measure changes in the separation distance between them. The KBR Assembly consists of a single horn antenna, an Ultra-Stable Oscillator (USO), frequency converters, and an Internal Processing Unit for both satellites (IPU).

Each satellite's front panel has the KBR-horn, which is used for both transmission and reception of microwave signals. Both satellites send out a dual microwave transmission with a carrier signal modified at 24 GHz K-Band and 32 GHz Ka-band frequencies.

The dual one-way range $R(t)$, which represents the distance between the centers of mass (CoMs) of the two satellites at a given time epoch t, is calculated as follows: (Kim and Tapley, 2002).

$$R(t) = \rho(t) + \Delta\rho_{TOF} + \Delta\rho_{Iono} + \Delta\rho_{AOC} + B + \Delta\rho_{err} \tag{2.41}$$

The instantaneous biased range at time epoch t is denoted by $R(t)$. The light-time correction $\Delta\rho_{TOF}$ compensates for the movement of the satellites during the signal time of flight (TOF). The ionospheric correction $\Delta\rho_{Iono}$is a method of adjusting the ionospheric pressure and is responsible for the ionospheric delay.

The antenna center offset correction $\Delta\rho_{AOC}$, sometimes known as antenna offset correction (AOC), is the distance between the KBR antenna phase center and the center of mass (CoM). The range bias B in one-way phases is caused by uncertain phase ambiguity values. And $\Delta\rho_{err}$ denotes measurement noise. Numerical differentiation of range measurements yields range rates and range accelerations. (Thomas, 1999) and (Kim, 2000), have more information on the KBR.

In-Orbit Constellation - Formation Keeping

Since inter-satellite range takes place between the two KBR horn antennas on every satellite's front panel, the leading satellite is continually turned one hundred eighty degrees around its z-axis. The KBR measuring methodology desires the KBR antenna section centers to be between some milliradians of the Line-Of-Sight (LOS). The formation flying needs a pitch angle offset of between 0.4° and 2.2°, depending on the altitude and spacing, to confirm a LOS orientation of the KBR microwave link (Kirschner et al., 2001). Each satellite flies with a 1° pitch angle offset at nominal altitude and separation to allow precise inter-satellite pointing between the two satellites. (cf. Fig. 2.6).

2.6.4 Data levels

A distributed Science data system (SDS) distributes and archives all accessible GRACE data outputs. The JPL, CSR, and GFZ collaborate on system development, science data processing, archiving, dissemination, and products verification (Case et al., 2010). The GRACE Level-0 through Level-2 SDS data packages are outlined as follows (Case et al., 2010):

Level-0:

The raw data Center (RDC) of the Mission Operation System (MOS), which is a component of the DLR and placed in Neustrelitz, Germany, collects and decommutates the raw science instrument and housekeeping data received from the GRACE satellites. The DLR is responsible for not simply data reception but additionally mission management for the GRACE satellites.

Level-1A:

The Level-1A data product is the result of a non-destructive process of the level 0 data that involves changing binary encoded measurements to engineering units.

Written material and internal control flags, yet as auxiliary data products needed for Level-1A to Level-1B processing, are included within the Level-1A data products.

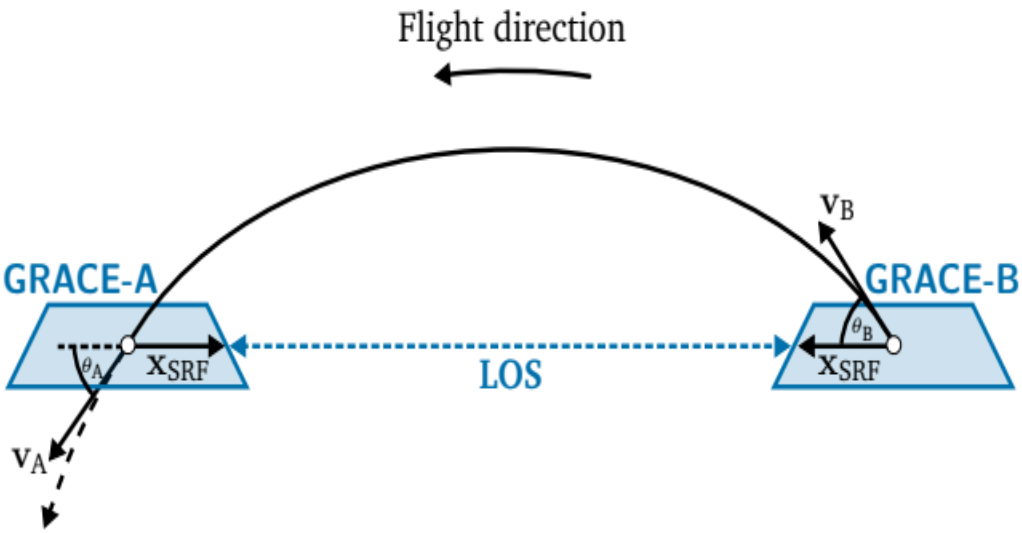

Figure 2.6 In-orbit constellation of the GRACE satellites: orientation of the leading and trailing satellite relative to the orbit trajectory, with a pitch angle offset (θ_A, θ_B) enabling KBR inter-satellite ranging. Source(Kvas et al., 2019)

Level-1B:

The Level-1B data product is generated from the Level-1A data products and comprises the ultimate and publicly accessible science instrument and housekeeping data products. The data is appropriately time-tagged, resampled, and translated to a shared organization throughout Level-1A to Level 1B data processing, thus the initial data cannot be reconstructed.

Level-2:

The Level-2 data product is created from the Level-1B data products and comprises the static and time-variable (monthly) gravity field models during a spherical harmonic form. Auxiliary data products (e.g., mean atmospheric and oceanic mass fluctuations) are enclosed within the Level-2 data products that are needed to evaluate temporal variations within gravity field solutions.

Chapter Three

Methodology

3.1 Software Used

The software for gravity field analysis, GROOPS (**GR**avity field **O**bject **O**riented **P**rogramming **S**ystem), includes all of the concepts and computation processes presented and used in this study. GROOPS is written in C++ and has an object-oriented design, which means that it is totally modular. This suggests a high level of adaptability in dealing with the numerous duties required in a gravity field recovery procedure.

GROOPS is an independent scientific software suite dedicated to all types of gravity field recovery and GNSS processing applications. Aside from that, the software provides a wide range of data management, conversion, and visualization functions in general. Prof. Dr.-Ing. Mayer-Gürr of the Institute of Geodesy and Geoinformation at the University of Bonn in Germany originally developed the software. The GROOPS software package has been maintained and developed by the Working Group for Theoretical Geodesy and Satellite Geodesy at the IfG at the Graz University of Technology since 2011. As a result, the software is always being developed and improved.

The GROOPS software now has around 400 distinct C++ routines. A Graphical User Interface (GUI) makes it easier to use software by providing pull-down menus that logically represent the major programs. Extensible Markup Language (XML) is used to create the user interface. The gravity field recovery from several satellite missions, such as GRACE, Champ, GOCE, or Swarm, is the principal field of application. The GROOPS software's highly modular design provides not just flexibility for various processing scenarios, but also detailed control over all important processing options.

It also provides a powerful platform for automating mission-specific processing chains. Several C++ routines for GRACE instrument and housekeeping data handling and data pre-processing were developed as part of this project. GROOPS are used to base all of the analysis and results.

3.2 Data and Sources

3.2.1 Level-1B data products

The GRACE release 02 (RL02) Level-1B data product indicated in Table 3.1 was used for the study and the results given during this thesis. In addition, the gravity field recovery uses pre-processed Level-1B data products and kinematic orbits generated using the raw acceleration technique (Zehentner and Mayer-Gürr, 2016).

Table 3.1: Overview of GRACE Level-1B science instrument and housekeeping data products

Science data product	**Description**
ACC1B	Accelerometer Data Product
GNV1B	GPS Navigation Data Format Record
KBR1B	KBR Data Format Record
SCA1B	Star Camera Data Product
Housekeeping data product	**Description**
THR1B	Thrusters Data Format Record

In general, two types of GRACE Level-1B data products are distinguished:

- Science data products, and
- Housekeeping data products.

The former is the data packages that are primarily employed by the scientific community since they provide crucial observations from the GRACE devices. The latter provides more data within the kind of internal satellite and/or telemetry data. The GRACE Level 1B data Product User handbook could be a full rationalization of the official Level-1B data product (Case et al., 2010).

3.2.1.1 Science Data Products

All GRACE Level-1B science data products refer to the satellite body-fixed Science Reference Frame (SRF). The data is sampled at a rate of 5 seconds, except for the ACC1B data (1 second) and the GNV1B data (60 seconds).

K-Band Ranging Data (KBR1B)

The KBR1B data product provides the dual-one-way ranging data (biased range, range rate, range acceleration), the light time correction, and therefore the geometric correction. The ranging data, contained within the KRB1B data product, must be corrected for these two effects, however, is already corrected for ionospheric effects. In addition, the signal-to-noise ratio (SNR) numbers of the K-/Ka-Band for GRACE-A and GRACE-B are provided, giving information concerning the signal strength and ranging measuring quality.

Accelerometer Data (ACC1B)

The ACC1B data product provides the linear and angular acceleration components (along-track, cross-track, radial) of the accelerometer-proof mass. The accelerations in the ACC1B data output include an instrument scale and bias offset since the accelerometer has an unknown scale and bias in every direction.

Star Camera Data (SCA1B)

The SCA1B data product gives attitude quaternions, describing the orientation of the GRACE satellites concerning the inertial frame.

Orbit Data (GNV1B)

The GNV1B data product provides the navigation solution for the GRACE satellites in terms of satellite positions and velocities according to the International Terrestrial reference frame (ITRF). Additionally, formal errors for each position and velocities are provided.

3.2.1.2 Housekeeping Data Products

Besides the GRACE science data product, auxiliary housekeeping data products are provided (cf. Tab. 3.1). Housekeeping data products comprise internal satellite data and/or telemetry data, that is required for the maintenance of the satellite instruments or the attitude and altitude control. The Level-1B housekeeping data products contain further information concerning the instrument health, the output of additional onboard sensors (e.g., temperature), or calibration data. Hence, it is a supplementary source of data to monitor the GRACE satellites and therefore helps analyze the GRACE science data.

Thruster Data (THR1B)

The THR1B data product contains the thruster activation data of the onboard cold-gas thrusters (7 pairs in total), individually for each satellite. The cold-gas thrusters are required for orbit and attitude control and are nominally operated in pairs. For every cold-gas thruster all thruster firing events are logged, as well as the precise activation time, and the length of every thruster activation.

3.3 Level-1B Data Pre-Processing

The GRACE Level-1B pre-processing may be seen as an a priori processing of the official GRACE Level-1B RL02 data products before they are used as input for the actual recovery of the gravity field.

3.3.1 Data Resampling

The Level-1B science data products are resampled to ensure a common sampling interval of 5 seconds and to interpolate tiny data gaps (up to a most predefined time interval). Table 3.2 gives a summary of the resampling technique used for the interpolation of accelerometer, orbit, and star camera data.

Table 3.2 Level-1B data resampling

Data product	Max. data gap	Resampling method
ACC1B	10s sec	Polynomial interpolation(degree=1)
SCA1B	10 min	Polynomial interpolation (degree=1)

3.3.2 Data Screening

The purpose of data screening before the particular data pre-processing is to automatically notice giant blunders and outliers among the Level-1B science data products. The data screening used in this study is threshold-based outlier detection tailored to the (accuracy) characteristics of the various science data products (Kvas et al., 2019).

Threshold-based outlier detection

Within the Level-1B data pre-processing, a completely automatic threshold-based outlier detection is done to reduce the number of blunders and huge outliers within the Level-1B data products.

The thresholds are defined through empirical observation consistent with the accuracy characteristics of the individual data products.

Depending on the instrument type and also the data products available, one (or more) of the subsequent methods can be applied:

1) median-based: $\left|x^i - \tilde{x}\right| \geq threshold$
2) absolute value: $\left|x^i\right| \geq threshold$
3) reference data: $\left|x^i - x^i_{ref}\right| \geq threshold$

Therein, x^i denotes arbitrary data derived from Level-1B data products at an epoch i, x^i_{ref} denotes reference data at constant epoch i and $\tilde{x}$ represents the median value of the data set. Methods (1) and (2) are chosen for data screening of Level-1B data products with no reference data available, i.e. the outlier detection is based on the data itself. Blunders within the data are identified using extreme values (1) or by deviations from the median value (2). With additional reference data available, outliers are identified by analyzing the differences between the data sets (3). The corresponding epochs are eliminated if the differences exceed a predetermined threshold.

An arbitrary margin will be set for all three approaches to remove epochs before and after the discovered outliers.

Table 3.3 level1B data screening: Threshold-based outlier detection(source(Kvas et al., 2019))

Data product	Data type	Threshold	Margin
ACC1B	Linear accelerations	$\left\|a^i_x - \tilde{a}_x\right\| \geq 10^{-5}$ $\left\|a^i_y - \tilde{a}_y\right\| \geq 10^{-5}$ $\left\|a^i_z - \tilde{a}_z\right\| \geq 10^{-5}$	600sec 600sec 600sec
ACCCalib, ACCModeled	Linear accelerations	$\left\|a^i_{x,calib} - a^i{}_{x,modeled}\right\| \geq 10^{-6}$ $\left\|a^i_{y,calib} - a^i{}_{y,modeled}\right\| \geq 10^{-6}$ $\left\|a^i_{z,calib} - a^i{}_{z,modeled}\right\| \geq 10^{-6}$	150sec 150sec 150sec

3.3.3 Accelerometer Data Calibration

Each GRACE satellite is equipped with space accelerometers measuring the non-gravitational accelerations acting upon them (Touboul et al., 1999). These forces are because of atmospheric drag, radiation pressure, and albedo.

The inter-satellite range measurements, which are carried out with micrometer precision by the onboard KBR system, are the main observables for GRACE's gravity field recovery (Kim, 2000). For the aim of gravity field recovery, the effects induced by the gravitational and non-gravitational forces need to be separated. As a result, accelerometer data are critical because they provide information about the non-gravitational forces that act on the two satellites. The accelerometer data, on the other hand, cannot be used directly and must be corrected since it contains instrument-specific bias and scale. Modeled non-gravitational accelerations serve as input for the calibration approach. The modeled forces are compared to the accelerometer measurements.

Calibration Approach

The linear accelerations contained within the ACC1B data product include an instrument scale and bias offset (i.e. subject to instrument-specific scale factors, biases, and random noise). The GRACE Technical Note TN-02 contains a general recommendation for the first estimation of the bias and scale parameters, which can be applied to the linear ACC1B data (Bettadpur, 2009). Many methodologies for GRACE accelerometer data calibration using POD(Precise Orbit Determination) generated accelerations have been implemented over the years (e.g., Bezdk, 2010). Throughout gravity field recovery, however, totally different parameterizations for bias and scale parameters and/or empirical parameters are employed by the various analysis centers. Consequently, the estimated calibration parameters and therefore the recovered gravity field solutions can vary a lot, depending on the utilized calibration technique and the context of data usage.

The approach used in this study is making use of modeled accelerometer data. The approach is schematically depicted in Fig. 3.1. In the first step, the modeled non-gravitational accelerations serve as a reference for the initial calibration of the original ACC1B data and are used for data screening purposes. By estimating the calibration parameters, the difference between the modeled and therefore calibrated accelerometer data is reduced (accelerometer biases and scale factors). This successively permits a data screening step at the Level-1B data preprocessing, because the modeled data is a reference for threshold-based outlier detection.

Data that has been affected by thruster firing events (given by the THR1B data product) is not considered throughout the a priori calibration. Therefore, the thruster-affected data and a few extra seconds of information before and after the thruster firing events are excluded.

Because the thruster firings are not modeled, these epochs are removed from the calibration procedure to avoid inaccurate calibration and outlier detection. It's worth noting that this calibration method attempts to eliminate the impact of instrument defects on gravity field recovery.

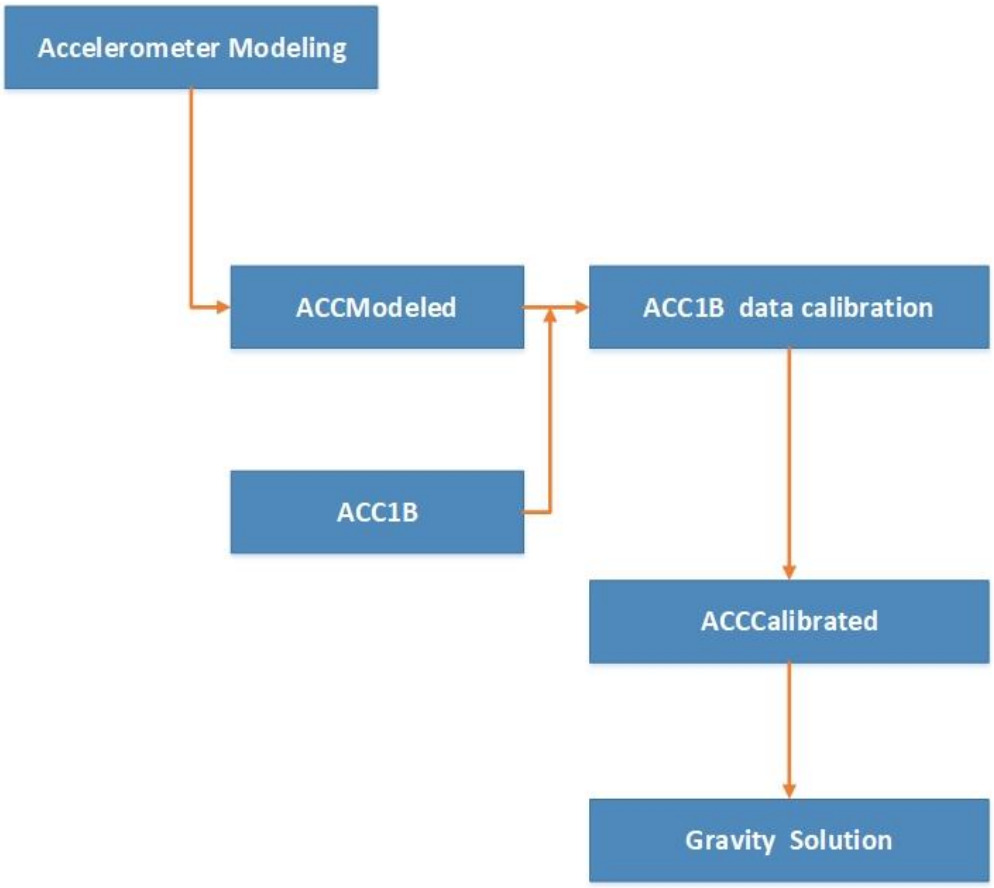

Figure 3.1 ACC1B data calibration approach

Calibration Equation

The ACC1B data product's linear accelerometer measurements are affected by unknown scale factors, biases, and random noise (Kim, 2000). Both accelerometer biases and scale factors are estimated on daily basis. The ACC1B data calibration relies on the subsequent calibration equation.

$$\boldsymbol{a_{cal}} = \boldsymbol{S a_{obs}} + \boldsymbol{b} \tag{3.1}$$

where, $\boldsymbol{a_{cal}}$ denotes the calibrated non-gravitational accelerations in the SRF, and $\boldsymbol{a_{obs}}$ denotes the initial accelerometer measurements (given by ACC1B). The 3x3-scale factor matrix $\boldsymbol{S}$ multiplies the observed accelerations, and the bias vector $\boldsymbol{b}$ is added.

Scale factors

Ideally, the scale factor matrix S should be an identity matrix with unity main diagonal elements and zero off-diagonal elements. But due to small instrument imperfections, which cause a mutual influence of the accelerometer axes among each other, it contains non-unit diagonal elements and non-zero off-diagonal elements. Fig. 3.5 illustrates possible accelerometer imperfections. To account for these small imperfections, the calibration equation presented in Eq.(3.1) uses a fully-populated scale factor matrix.

The scale factor matrix is composed of both diagonal and off-diagonal elements. The diagonal elements $\boldsymbol{s_x}, \boldsymbol{s_y}, \boldsymbol{s_y}$ influence the magnitude of the measured acceleration components in along-track, cross-track, and radial direction, respectively. The initial misalignment is due to a misfit in the spacecraft's accelerometer installation (Kim, 2000). As a result, the accelerometer axes (AF) do not line up properly with the spacecraft coordinates (SRF).

$$\mathbf{S} = \begin{bmatrix} s_x & \alpha + \zeta & \beta - \varepsilon \\ \alpha - \zeta & s_y & \gamma + \delta \\ \beta + \varepsilon & \gamma - \delta & s_z \end{bmatrix} \tag{3.2}$$

3.4 Background Models

All other forces acting on the satellite must be reduced before the gravitational field of the Earth can be derived from satellite data. These disturbing forces can be estimated using appropriate models or measured using the onboard accelerometer. The following is a summary of the background models among those used in this study. All the models used in this study are provided publicly by Kvas et al., (2019).

Direct Tides

The satellite's orbit is influenced by tidal forces from the sun, moon, and planets in addition to the gravitational pull of the Earth. The differences in gravitational forces between third bodies acting on the Earth and the satellite are known as tidal forces.

Ocean Tides

The oceanic response to tidal forces and the gravitational effects that arise are modeled.

Solid Earth Tides

The above-mentioned tidal forces cause the Earth to deform. This causes mass displacements, causing a change in the solid Earth's gravitational potential, known as tidal potential.

Pole Tides

The centrifugal force of polar motion causes a deformation of the Earth and hence a change in the gravitational potential, resulting in polar tides.

De-aliasing

Short periodic variations in air masses, as well as the ocean's reaction to these mass variations, must be modeled and reduced, or the solution will be distorted by aliasing effects. As a result, de-aliasing data models are used to account for small periodic fluctuations (AOD1B).

Non-gravitational Forces

The satellite's gravitational and non-gravitational forces must be separated. Because models can't simply simulate them, the satellite's onboard accelerometer in the center of mass must be used to measure them directly. The non-gravitational forces include surface forces such as atmospheric drag, solar radiation, and Earth albedo, as well as accelerations generated by guiding thrusters.

3.5 Setup of Mathematical Model

The purpose of the satellite missions (i.e CHAMP, GRACE, and GOCE) is to see the earth's gravity field as accurately as possible. As a result, a link between the (unknown) gravitational field parameters and the presented observations must be constructed. This can be obtained via a practical model that links the actual observations to the gravity field parameters. We have a (linearized) system of equations that can be solved using a least-squares adjustment process when we combine the observation equations at different observation times.

The gravity field recovery approach tailored to a twin satellite gravity mission of the GRACE sort mentioned in the literature review (c.f chapter 2), relies on Newton’s equation of motion, developed as a boundary value problem within the type of a Fredholm type integral equation.

This concept has been projected as a general technique for orbit determination by Schneider in 1967 (Schneider, 1968), modified for gravity field determination by (Schneider and Reigber, 1970), investigated well by (Reigber, 1969), and with success applied subsequently. Following, the concept has been applied to the satellite-to-satellite tracking (SST) problem (Ilk, 1984) and later to the satellite gravity gradiometry (SGG) analysis. After that, the technique has been advanced and examined primarily based totally on numerous simulation scenarios, e.g. see (Thalhammer et al., 1995).

As the first real data applications, the gravity field models ITG-CHAMP01 and ITG-CHAMP02 were derived primarily based totally on this technique, implemented in the analysis of kinematical short arcs (Mayer-Gürr et al., 2005). The primary characteristic of this technique is the usage of short arcs for local and global gravity field recovery applications. The whole recovery system includes three steps which may be implemented independently as well (Mayer-Gürr et al., 2006).

- Global gravity field recovery based on a spherical harmonic expansion up to a moderate degree to provide a first global reference model as a basis for further refinements,
- Regional refinements of the gravity field by spherical splines as space localizing base functions, adapted to the specific gravity field features, if possible covering the globe,
- Determination of a global gravity field model by merging the regional refinement solutions and deriving potential coefficients by a numerical quadrature technique.

3.5.1 The Equation of Relative Motion for Twin Satellites

If precise inter-satellite functionals such as line-of-sight ranges or range-rate measurements are available, as they are with the GRACE mission, the mathematical model can be based on Newton's equation of motion for line-of-sight distance. From Newton's equation of relative motion,

$$\ddot{\boldsymbol{r}}_{12}(t) = \boldsymbol{g}(t; \boldsymbol{r}_{12}, \boldsymbol{r}_1, \dot{\boldsymbol{r}}_1, \dot{\boldsymbol{r}}_2; \boldsymbol{x}) \tag{3.3}$$

formulated as a boundary value problem,

$$r_{12} = (1-\tau) r_{12,A} + \tau r_{12,B} - T^2 \int_{\tau'=0}^{1} K(\tau, \tau') \left(\frac{\dot{\boldsymbol{r}}_{12}^2 - \dot{r}_{12}^2}{r_{12}} + e_{12} \cdot \boldsymbol{g}(t; \boldsymbol{r}_{12}, \boldsymbol{r}_1, \dot{\boldsymbol{r}}_1, \dot{\boldsymbol{r}}_2; \boldsymbol{x}) \right) d\tau'. \tag{3.4}$$

The quantity $K(\tau, \tau')$ is the integral kernel,

$$K(\tau,\tau') = \begin{cases} \tau(1-\tau'), & \tau \le \tau', \\ \tau'(1-\tau), & \tau' \le \tau, \end{cases}$$

with the normalized time variable,

$$\tau = \frac{t-t_A}{T} \quad \text{with} \quad T = t_B - t_A, \quad t \in [t_A, t_B].$$

$$r_{12,A} := r_{12}(t_A), \quad r_{12,B} := r_{12}(t_B), \qquad t_A < t_B$$

The relative velocity can be derived by differentiation with respect to the time,

$$\dot{r}_{12}(t) = \frac{1}{T}\left(r_{12,B} - r_{12,A}\right) - T \int_{\tau'=0}^{1} \frac{dK(\tau,\tau')}{d\tau}\, g(\tau'; r_{12}, r_1, \dot{r}_1, \dot{r}_2; x) d\tau' \tag{3.5}$$

The mathematical model for range observations can be derived by projecting the relative vector to the line-of-sight connection in combination with Eq. (3.4)

$$r_{12}(t) = e_{12}(\tau) \cdot \boldsymbol{r}_{12}(\tau) \tag{3.6}$$

Analogously, the mathematical model for range-rate measurements in combination with Eq. (3.5) read as follows,

$$\dot{r}_{12}(t) = e_{12}(\tau) \cdot \dot{\boldsymbol{r}}_{12}(\tau) \tag{3.7}$$

In both equations, e_{12} is the unit vector in the line-of-sight direction (Fig. 2.6). This vector may be calculated with high precision if the satellite locations are estimated to be within a few centimeters and the distance between the two satellites is about 200 km. For the above model's alternatives, the normal equations will be established and solved by a regularized solver of the Tikhonov type, where the regularization parameter is ideally computed according to the variance component estimation procedure (Koch and Kusche, 2002).

3.5.2 Gravity Field Representation

The specific force function,

$$g(\tau'; r_{12}, r_1, \dot{r}_1, \dot{r}_2; x) = g_d(\tau'; r_1, r_2, \dot{r}_1, \dot{r}_2) + \nabla V_{(12)E}(\tau'; r_{12}, r_1; x_0) + \nabla T_{(12)E}(\tau'; r_{12}, r_1; \Delta x) \tag{3.8}$$

with the gravity field parameters, x can be separated in a disturbance part g_d, which represents the non-conservative disturbing forces, in a reference part $\nabla V_{(12)E}$, modeled by the tidal potential of the Earth (E) acting on the satellites 1 and 2,

$$\nabla V_{(12)E}(\tau'; \boldsymbol{r}_{12}, \boldsymbol{r}_1; \boldsymbol{x_0}) = \nabla\big(V(\boldsymbol{r}_1 + \boldsymbol{r}_{12}) - V(\boldsymbol{r}_1)\big) \tag{3.9}$$

Representing the long-wavelength gravity field features and in an anomalous part $\nabla T_{(12)E}$,

$$\nabla T_{(12)E}(\tau'; \boldsymbol{r}_{12}, \boldsymbol{r}_1; \Delta\boldsymbol{x}) = \nabla\big(T(\boldsymbol{r}_1 + \boldsymbol{r}_{12}) - T(\boldsymbol{r}_1)\big) \tag{3.10}$$

Modeling the high frequent refinements and parameterized either by corrections $\Delta\boldsymbol{x}$ to the global gravity field parameters $\boldsymbol{x_0}$ or by parameters $\Delta\boldsymbol{x}$ of a linear approximation with space localizing base functions. Anomalous potential according to Eq. (3.10), in case of a regional recovery the anomalous potential $T(r)$ is modeled by parameters of space localizing base functions,

$$T(\boldsymbol{r}) = \sum_{i=1}^{I} a_i \, \varphi\big(\boldsymbol{r}, \boldsymbol{r}_{Q_i}\big), \tag{3.11}$$

With the unknown field parameters a_i arranged in a column matrix, $\boldsymbol{\Delta x} := (a_i, i = 1, \dots, I)^T$ and the base functions,

$$\varphi\big(\boldsymbol{r}, \boldsymbol{r}_{Q_i}\big) = \sum_{n=0}^{N_{max}} k_n \, \left(\frac{R_E}{r}\right)^{n+1} P_n\big(\boldsymbol{r}, \boldsymbol{r}_{Q_i}\big) \tag{3.12}$$

The coefficients k_n are the difference degree variances of the gravity field spectrum to be determined minus the reference gravity field ($\Delta\bar{c}_{nm}^2$, $\Delta\bar{s}_{nm}^2$ are the fully normalized potential coefficients),

$$k_n = \sum_{m=0}^{n} (\Delta\bar{c}_{nm}^2 + \Delta\bar{s}_{nm}^2) \tag{3.13}$$

R_E is the mean equator radius of the Earth, r the distance of a field point from the geo-center, and $P_n(\boldsymbol{r}, \boldsymbol{r}_{Q_i})$ are the Legendre polynomials depending on the spherical distance between a field point P and the nodal points Q_i of the set of base functions. The maximum degree N_{max} in Eq. (3.12) should correspond to the envisaged maximum resolution expected for the regional recovery.

3.5.3 Least Squares Estimation

The method for estimating unknown gravitational field parameters from a set of observations will be detailed in the following sections. As explained by (Koch, 1999), this estimation method is a conventional Gauss-Markoff-Model. A vector y of the dimension $n\ x\ 1$ is frequently used to organize all n observations. A column vector x with the dimension $u\ x\ 1$ can likewise be used to combine u unknown parameters. The observations can be linked to the unknown parameters using a functional model $f(\bar{x})$, and the model can then be constructed using this model and an extra measurement ϵ noise,

$$\bar{y} = f(\bar{x}) + \epsilon \tag{3.14}$$

If the model is non-linear, linearization is unavoidable; therefore, estimated values for unknown parameters must be added, and approximate observations will be produced as functions of the approximate values. In the case of a linear model, it is recommended to start with approximate values for the unknown parameters as well and to calculate their influence on the observations,

$$y_0 = f(x_0) \tag{3.15}$$

The linearization procedure of the model f with respect to the unknown parameters can be performed by a Taylor expansion truncated after the linear term,

$$\bar{y} = y_0 + \left.\frac{\partial f(\bar{x})}{\partial \bar{x}}\right|_0 (\bar{x} - x_0) + \ldots \tag{3.16}$$

The reduced observations and the corrections to the unknown parameters are then calculated according to,

$$\mathrm{y} = \bar{y} - y_0 \quad \text{and } x = \bar{x} - x_0 \tag{3.17}$$

The partial derivatives of the linearization Eq. (3.16) can be combined in the design matrix A. It is of dimension $n\ \times\ u$, and its elements are defined by the partial derivatives of the function $f_k(x)$ with respect to x_i,

$$(A)_{ki} = \left.\frac{\partial f_k(\bar{x})}{\partial x_i}\right|_0 \tag{3.18}$$

The result is a linear system of equations,

$$\boldsymbol{y} = \boldsymbol{A}\boldsymbol{x} + \epsilon \qquad \text{with} \qquad \mathcal{C}(\epsilon) = \sigma^2 \boldsymbol{P}_\epsilon^{-1} \tag{3.19}$$

The conventional Gauss-Markov model is based on the assumptions that measurement errors have a zero expectation and that the data' covariance matrix is known a priori.

$$E\{\epsilon\} = \mathbf{0} \text{ and } \mathcal{C}(\epsilon) = \mathcal{C}(y) = \sigma^2 \boldsymbol{P}_\epsilon^{-1} \tag{3.20}$$

The unknown variance factor is denoted by σ, while the weight matrix of the observations is denoted by $\boldsymbol{P}_\epsilon$. The minimization of the square sum of the residuals corresponds to a least-squares adjustment estimation.

$$\Omega = \frac{1}{\sigma^2} (\boldsymbol{y} - \boldsymbol{A}\boldsymbol{x})^T \boldsymbol{P}_\epsilon (\boldsymbol{y} - \boldsymbol{A}\boldsymbol{x}) \tag{3.21}$$

Differentiation according to the minimum condition can be achieved by,

$$\frac{\partial \Omega}{\partial \hat{\boldsymbol{x}}} = 2\boldsymbol{A}^{\boldsymbol{T}} \boldsymbol{P}_{\boldsymbol{\epsilon}} \boldsymbol{A}\boldsymbol{x} - 2\boldsymbol{A}^{\boldsymbol{T}} \boldsymbol{P}_{\boldsymbol{\epsilon}} \boldsymbol{y} = 0 \tag{3.22}$$

As a result, the following system of normal equations emerges,

$$\boldsymbol{N}\boldsymbol{x} = \boldsymbol{n} \quad \text{with} \quad \boldsymbol{N} = \boldsymbol{A}^{\boldsymbol{T}} \boldsymbol{P}_{\boldsymbol{\epsilon}} \boldsymbol{A}\boldsymbol{x} \text{ and } \boldsymbol{n} = \boldsymbol{A}^{\boldsymbol{T}} \boldsymbol{P}_{\boldsymbol{\epsilon}} \boldsymbol{y} \tag{3.23}$$

The least-squares adjustment is used to estimate the unknown parameters after solving the normal equations.

$$\hat{\boldsymbol{x}} = (\boldsymbol{A}^{\boldsymbol{T}} \boldsymbol{P}_{\boldsymbol{\epsilon}} \boldsymbol{A})^{-1} \boldsymbol{A}^{\boldsymbol{T}} \boldsymbol{P}_{\boldsymbol{\epsilon}} \boldsymbol{y} = \boldsymbol{N}^{-1} \boldsymbol{n} \tag{3.24}$$

The likelihood function is maximized as a result of this solution, which corresponds to the best linear unbiased estimate (Koch, 1999). The law of covariance propagation can be used to derive the covariance matrix of the unknown parameters $\mathcal{C}(\hat{x})$,

$$\mathcal{C}(\hat{x}) = \sigma^2 N^{-1} \tag{3.25}$$

The unknown variance factor can be calculated using the formula,

$$\hat{\sigma} = \frac{1}{n-u} (\boldsymbol{y} - \boldsymbol{A}\hat{\boldsymbol{x}})^T \boldsymbol{P}_\epsilon (\boldsymbol{y} - \boldsymbol{A}\hat{\boldsymbol{x}}). \tag{3.26}$$

It yields the unknown parameters' estimated covariance matrix,

$$\hat{\mathcal{C}}(\hat{x}) = \hat{\sigma}^2 N^{-1}. \tag{3.27}$$

3.5.4 Variance Component Estimation (VCE)

When combining different types of observations, determining the proper relative weighting of the observations is critical to obtaining a correct result. Within the same context, the choice of the regularization parameter can be treated. The approach of variance component estimation (VCE), as explained by (Koch and Kusche, 2002), was used for both tasks. A system of (combined) normal equations N that is accumulated as a weighted sum of the normal equation systems N_k of the different observation groups can be used to estimate the solution. This can be expressed as follows:

$$\boldsymbol{N}\hat{\boldsymbol{x}} = \boldsymbol{n} \quad \text{with} \quad \boldsymbol{N} = \sum_k \frac{1}{\sigma_k^2} \boldsymbol{N}_k \quad \text{and} \quad \boldsymbol{n} = \sum_k \frac{1}{\sigma_k^2} \boldsymbol{n}_k \tag{3.28}$$

The reciprocal variances of the normal equations are used as weighting factors.

$$\hat{\sigma}_k^2 = \frac{\Omega_k}{r_k} \tag{3.29}$$

with

$$\Omega_k = \hat{e}_k^T \, P_k \, \hat{e}_k = \, (A_k \hat{x} - l_k)^T P_k (A_k \hat{x} - l_k) \tag{3.30}$$

being the square sum of the kth group of observations' residuals and

$$r_k = n_k - \frac{1}{\sigma_k^2} trace(N_k \, N^{-1}) \tag{3.31}$$

their partial redundancy with n_k denoting the number of observations in the k^{th} group. The total redundancy is the sum of the partial redundancies, $\sum_k r_k = n - u$. The solution $\hat{x}$ and the variances σ_k^2 are unknown apriori. The following system results from the described approximation of the regularization matrix by the unit matrix.

$$N = \frac{1}{\sigma_\epsilon^2} \, A^T P_\epsilon A + \frac{1}{\sigma_s^2} \mathrm{I} \quad \text{and} \quad n = \frac{1}{\sigma_\epsilon^2} A^T P_\epsilon l \tag{3.32}$$

where σ_ϵ is the standard deviation of the observations and σ_s is the standard deviation of the signal.

3.6 Solving the System of Observation Equations

The solution of the observation equations defined in Section 3.5 is the subject of this section. The solution is obtained using a least-squares adjustment, as described in Section 3.5.3.

The ill-posedness of the downward continuation technique, which is unavoidable when dealing with information from satellite altitude and seeking to determine the gravity field on the Earth's surface, is given special attention. The problem may be stabilized by the introduction of prior information to overcome the problems posed by the downward continuation. This corresponds to a regularization according to Tikhonov. The regularization parameter is set by a variance component estimation procedure.

3.6.1 Inverse Problems, Ill-Posed Problems

The concepts of inverse and ill-posed issues are crucial for dealing with geodetic problems, particularly in satellite geodesy. The subject has been widely explored in the geodetic community, for example, by Heiskanen and Moritz, (1967). As soon as any of these conditions (existence, uniqueness, and stability) according to (Hadamard, 1923), is violated, the problem is said to be an 'improperly posed' or 'ill-posed' problem.

In geodesy, inverse problems are common since the model parameters to be derived are rarely subject to direct observations. Inverse problems are frequently ill-posed, as at least one of the aforementioned conditions is frequently not met. The challenge of calculating the mass distribution in the interior of the Earth from the exterior gravitational potential, for example, is non-unique because infinitely numerous mass distributions can result in the same exterior gravity field. The calculation of gravity field functionals on the Earth's surface from measurements in satellite altitude causes an ill-posed problem, as during the downward continuation the signal is amplified especially in the high-frequency part of the spectrum.

3.6.2 Regularization

When it comes to least squares estimation, this means minimizing the square sum of the residuals,

$$J(x) = \frac{1}{\sigma_\epsilon^2}(Ax - y)^T P_\epsilon (Ax - y) := \|Ax - y\|^2_{C(\epsilon)} \tag{3.34}$$

does not result in a stable solution by itself. As a result, additional prior information on the solution must be provided. These are frequently apriori values for unknown parameters obtained from existing models, as well as smoothness assumptions in terms of an apriori given unknown parameter covariance matrix. Regularization refers to the process of stabilization.

Tikhonov Regularization

This method of regularization was developed separately by Tikhonov, (1963) and Phillips, (1962). The approach is based on the minimization of the functional Eq. (3.34) under consideration of a 'penalty term' $\|s\|_k^2$ that expresses the signal s's norm as a linear functional $\boldsymbol{Lx}$ with unknown parameters x,

$$\boldsymbol{s} = \boldsymbol{Lx} \tag{3.35}$$

$\|s\|_k^2$ represents a smoothing norm, such as the inner product of a reproducing kernel Hilbert space with kernel K as,

$$\|s\|_k^2 = \langle s, s \rangle_k \tag{3.36}$$

The requirement of this norm must be finite,

$$\|s\|_k^2 \leq c < \infty \tag{3.37}$$

does not only introduce a bound on the norm of the solution but, it also implies a smoothness constraint defined by the kernel K, which is equivalent to the smoothness assumption imposed by the RKHS kernel. The resulting functional to minimize Eq. (3.34) and Eq. (3.36) simultaneously can be formulated as follows,

$$J_\alpha(x) = \|Ax - y\|_{\mathcal{C}(\varepsilon)}^2 + \alpha\|s\|_k^2 \tag{3.38}$$

with α denoting the regularization or smoothing parameter. The minimization of Eq. (3.38) is a balance between minimizing the residual norm and maintaining the penalty term $\|s\|_k^2$ small. Small errors in the data cause huge variances in the solution due to the ill-posedness of the original model. To overcome this, the solution's norm must be limited.

The regularization parameter α in Eq. (3.38) is interpreted here as the signal-to-noise ratio,

$$\frac{1}{\alpha} = \frac{\sigma_s^2}{\sigma_\epsilon^2} \tag{3.39}$$

As a result, the regularized solution can be stated according to

$$x_\alpha = (A^T P_\epsilon A + \alpha L^T P_s L)^{-1} A^T P_\epsilon \, y. \tag{3.40}$$

In this case, x_α gives an unbiased least squares estimation of the unknown parameters (Eicker, 2008). The regularization parameter selection is critical because it resembles the trade-off between the solution's fit to the provided data set and the regularized solution's norm and smoothness. The dampening and smoothness of the solution increase as the regularization parameter is increased. The given signal will determine the parameter. The solution must be regularized as much as possible in order to obtain a reasonable result. But on the other hand, the signal should not be overly dampened in order to avoid losing any of the data's information. With the regularization matrix R, the functional $J_\alpha(x)$ and regularized solution for the minimization of the functional x_α is given by

$$J_\alpha(x) = (Ax - y)^T P_\epsilon (Ax - y) + \alpha \cdot x^T R\, x \tag{3.41}$$

$$x_\alpha(x) = (A^T P_\epsilon A + \alpha R)^{-1} A^T P_\epsilon y \tag{3.42}$$

For the regional refinement method, the regularization matrix is to be approximated by the unit matrix (Eicker, 2008). This has the advantage of allowing the regularization matrix to be separated and distinct matrices to be calculated for different areas. The approximation,

$$R = I \tag{3.43}$$

leads to the functional $J_\alpha(x)$ of Eq. (3.34) to be modified according to

$$J_\alpha(x) = (Ax - y)^T P_\epsilon (Ax - y) + \alpha \cdot x^T x \tag{3.44}$$

resulting in the regularized solution

$$x_\alpha(x) = (A^T P_\epsilon A + \alpha I)^{-1} A^T P_\epsilon y \tag{3.45}$$

3.7 General Gravity Recovery Methodological Workflow

The diagram below (Fig. 3.2) explains schematically the processing steps of the study by which the unknown parameters are estimated. Based on the GRACE Level-1B input data and background models, the monthly gravity field refinement was estimated in terms of the weighting coefficients by an iterative least-square estimation using the integral equation of the Fredholm type.

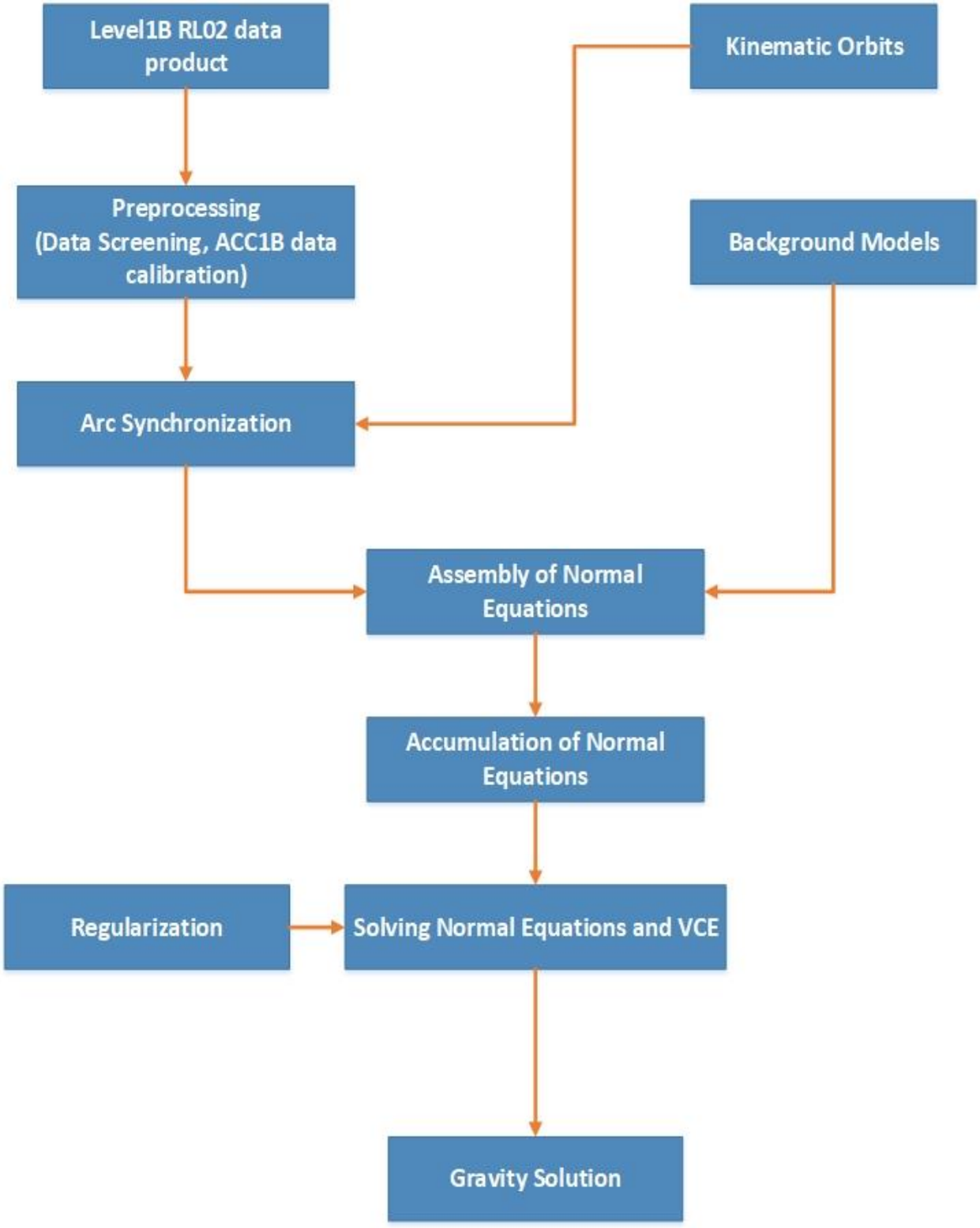

Figure 3.2 General Gravity Recovery Methodological Workflow

Chapter Four

Data Processing and Analysis

4.1 Accelerometer Data Calibration

Several scientific tasks and missions require detailed modeling and knowledge of non-gravitational forces acting on satellites. Since 2002, the twin GRACE spacecraft, now known as GRACE-FO, have been measuring these forces in low Earth orbit with highly precise accelerometers. Unfortunately, before any scientific use, the accelerometer measurements must be calibrated, with the scale factor and bias being estimated regularly (Wöske et al., 2019).

The requirement for very precise non-gravitational force modeling is rapidly growing. The increasing accuracy of measuring techniques and sensors necessitates a thorough examination and modeling of all physical processes affecting satellites. This encompasses not only gravitational forces but also all other forces originating from non-gravitational sources. These forces are derived from the Sun's, Earth's, and satellite's radiation, as well as residual atmosphere. Precise orbit determination (POD) methods need detailed force models for accurate orbit propagation and orbit determination from all sorts of measurement data (Jäggi et al., 2006). As a result, understanding non-gravitational forces, as well as enhanced modeling skills, is critical for a variety of activities involving precise satellite measurements. The gravitational field of a body is generated by the motion of satellites in this field, as an example in satellite geodesy. The non-gravitational forces acting on the satellites must be determined to determine just the gravitational effects. Because understanding non-gravitational accelerations is critical for gravity field recovery (GFR), accelerometers are used to measure them. The GRACE accelerometer data must be calibrated on a regular basis in order to be used (Srinivas Bettadpur, 2009; Van Helleputte et al., 2009).

The calibration methodology used in this study is based entirely on precisely modeled non-gravitational accelerations (Kvas et al., 2019), as shown in the methodology section. As a result, the accelerometer measurements were calibrated using modeled accelerations, and the residual was analyzed. The difference between calibrated accelerometer data and modeled accelerations is referred to as residuals.

4.1.1 Raw Accelerometer Data

At process level 1B (L1B), nearly all science sensor data from the two satellites is publicly available (Case et al., 2010). All satellite sensor data are presented within the science reference frame (SRF) that is installed on the satellite. The origin of that frame is located in the satellite's center of mass (CoM), the x-axis is perpendicular to the front panel of the satellite, the z-axis is perpendicular to the bottom panel, and the y-axis completes the right-hand system (Bettadpur, 2012). The satellite reference frame is shown in Fig. 4.1.

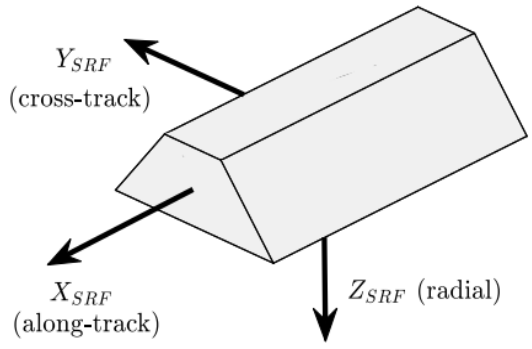

Figure 4.1 Sketch of a GRACE satellite with the body fixed science reference frame (SRF), with its origin at the CoM of the satellite. source (Wöske et al., 2019)

The GRACE satellites in science mode point their x-axis (line of sight direction) at one another and maintain this pointing with an accuracy of less than 0.5°. Two-star cameras measure the real attitude. Because of the 200-kilometer distance between the two spacecraft, the nominal flight path angle between them is roughly 1°, depending on which one is leading and which is trailing. Because the orbits of both satellites are not exactly the same, there is also a slight sideslip angle, which never surpasses 1°. As a result, drag is mostly operating in the X_{SRF} direction. The Y_{SRF} axis is sort of perpendicular to the orbital plane. $x-$, $y-$ and $z-axis$ are often referred to as along-track, cross-track, and radial direction, respectively. Leading and trailing satellites were switched two times at end of 2005 and in mid-2014.

The pattern of non-gravitational accelerations acting on the satellites is mostly governed by the orientation of the orbit with respect to the Sun, due to the practically constant attitude with respect to the orbital frame.

Calibration Equation

The calibrated, corrected accelerometer data $\boldsymbol{a_{cal}}$ for each accelerometer are given by,

$$\boldsymbol{a_{cal}} = \boldsymbol{S a_{obs}} + \boldsymbol{b} \tag{4.1}$$

with the scale factor vector $\boldsymbol{S}$ and bias vector $\boldsymbol{b}$.

This study employed a method of least squares estimates to calibrate the GRACE ACC1B data using the modeled non-gravitational accelerations a_{sim} as a reference. The calibration parameters for the daily mean are established. A shorter period might be more accurate for some days with large temperature changes in the accelerometer, but one day is acceptable for the majority of all epochs (Wöske et al., 2019). The raw ACC1B data is first filtered to remove any spikes induced by attitude thruster firings, which are not included in the modeled accelerations. A residual for each data point is determined as

$$\boldsymbol{r} = \boldsymbol{a_{cal}} - \boldsymbol{a_{sim}} \tag{4.2}$$

A root mean square (rms) residual $\boldsymbol{r_{rms,i}}$ for each axis i is computed from these residuals as a single measure for one day:

$$r_{rms,i} = rms(\boldsymbol{r}_i) \tag{4.3}$$

Fig. 4.2 depicts an example of modeled and calibrated accelerometer data with residuals for one day, (that is from January 2016). The modeled data agree extremely well with the GRACE data, particularly in the cross-track (y) and radial (z) directions, as seen by direct comparison and residuals with values of $r_{rms,y} = 0.72 nm/s^2$ and $r_{rms,z} = 0.55 nm/s^2$, respectively. When compared to the remainder of the two axes $r_{rms,x} = 1.90 nm/s^2$, the along-track (x) direction is not good enough.

The deficiency of atmospheric drag modeling, or more precisely, atmospheric density modeling, is thought to be the cause. The drag force is tightly aligned in this direction due to the dedicated satellites' attitude and shape. The radiation force sources and environmental fluctuations are better known and monitored, allowing for more precise modeling.

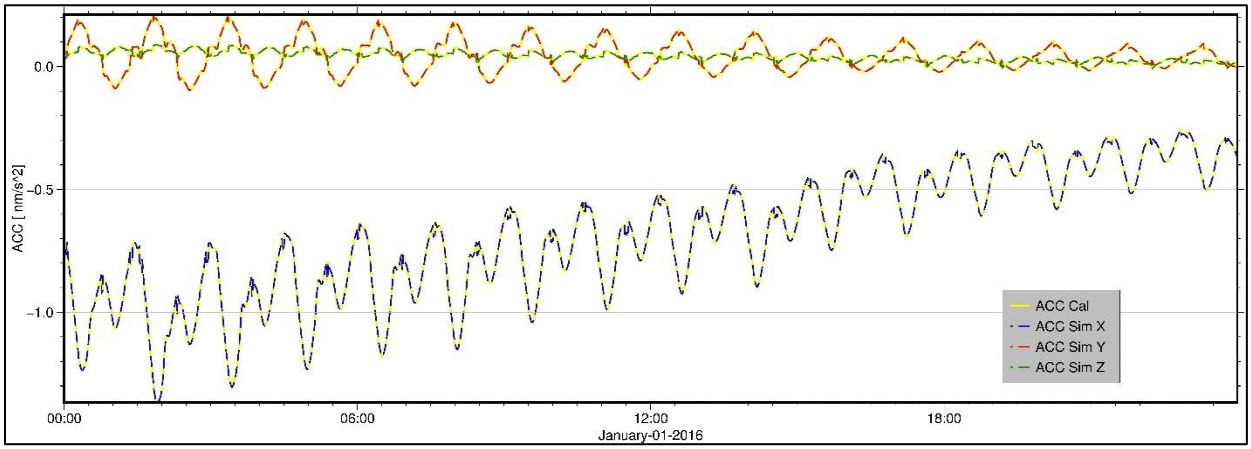

Figure 4.2 Calibrated ACC1B data ACC Cal with modeled non-gravitational accelerations ACC Sim from GRACE A. for January 01, 2016

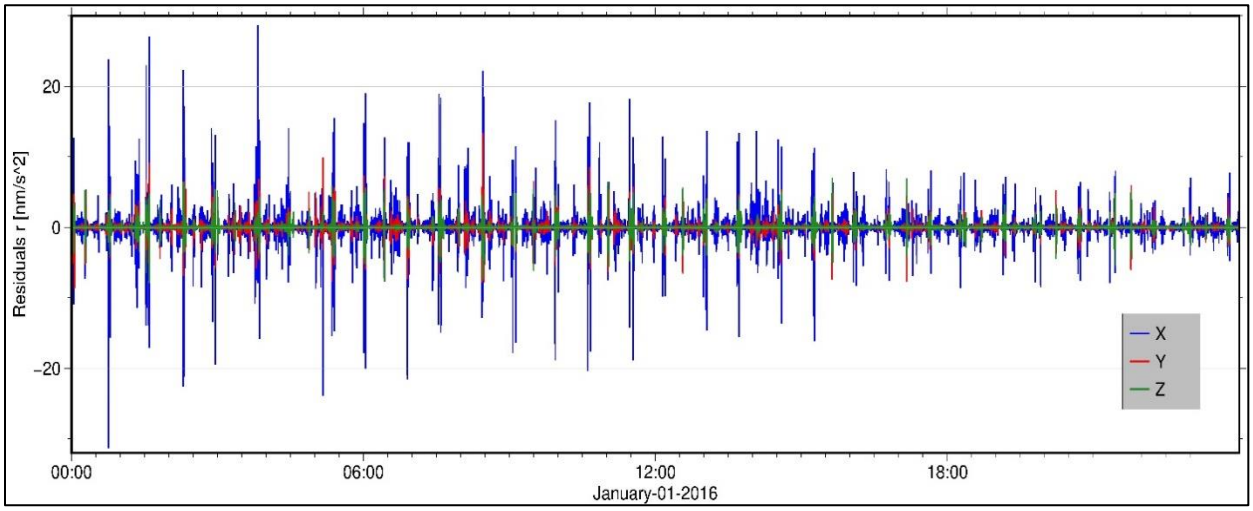

Figure 4.3 Resulting residuals of calibration for each axis.

4.2 Radial Basis Functions (RBFs) Parametrization

For the global solution, the potential is parameterized using spherical harmonics; however, for a regional gravity field recovery, the potential must be parameterized using space localizing basis functions. The spherical distance between two points on the sphere characterizes RBFs.

The radial symmetry of the basis functions $\varphi(\boldsymbol{r}, \boldsymbol{r}_{Q_i})$ allows them to be represented as a sum of Legendre polynomials. It is as follows, according to Eicker (2008) and Bentel et al. (2013):-

$$\varphi(\boldsymbol{r}, \boldsymbol{r}_{Q_i}) = \sum_{n=0}^{N_{max}} k_n \left(\frac{R_E}{r}\right)^{n+1} P_n(\boldsymbol{r}, \boldsymbol{r}_{Q_i}) \tag{4.5}$$

where $\boldsymbol{r}$ denotes the evaluation position and $\boldsymbol{r}_{Q_i}$ denotes the RBF space localization. The shape of the basis function is determined by the coefficients k_n. In general, the disturbing potential's functionals (see Sec. 2.2) may be written as the sum of a series expansion evaluated at a given point $\boldsymbol{r}$. It is as follows:

$$T(\boldsymbol{r}) = \sum_{i=1}^{I} a_i \, \varphi(\boldsymbol{r}, \boldsymbol{r}_{Q_i}), \tag{4.6}$$

where the unknown RBF weights a_i are included in this linear combination to be determined. The disturbing potential is a harmonic function. As a result, the RBFs are sometimes referred to as harmonic (Eicker, 2008). In a column matrix $\boldsymbol{\Delta x} := (a_i, i = 1, \dots, I)^T$, the unknown field parameters a_i are ordered. The difference degree variances of the gravity field spectrum to be computed minus the reference gravity field are the coefficients k_n ($\Delta\bar{c}_{nm}^2$, $\Delta\bar{s}_{nm}^2$ are the fully normalized potential coefficients),

$$k_n = \sum_{m=0}^{n} (\Delta\bar{c}_{nm}^2 + \Delta\bar{s}_{nm}^2) \tag{4.7}$$

These values are certainly unknown a priori in a regional gravity field refinement and must be estimated using a variance model. The so-called spline kernel, which takes into consideration the frequency response of the Earth's gravitational field, is one technique to establish the shape of the basis functions (see Eicker, 2008; Naeimi, 2013). The degree variances of a GGM reflect these responses. They may be estimated using spherical harmonic coefficients according to

$$\sigma_n^2 = \sum_{m=0}^{n} \bar{c}_{nm}^2 + \bar{s}_{nm}^2 \tag{4.8}$$

The approach of (Eicker, 2008) is used to estimate the scaling RBF coefficients in this study. The RBFs are defined using this approach according to Eq. (4.5), and the coefficients k_n are provided as,

$$k_n = \frac{\sigma_n}{\sqrt{2n+1}} \tag{4.9}$$

The k_n coefficients are important in affecting the shape of the basis functions because the Legendre polynomials' weighting is degree-dependent.

Up to a particular degree and order, the error degree variances σ_n^2, are given by an a priori has known GGM model. These error degree variances show the signal that is still there in the data. Taking this information into consideration implies that the GGM's accuracy information is included in the computing process, and the solution is regularized towards this prior information.

The EGM96 model error degree variances up to degree and order 120 were considered in this study. The GGM does not give full-spectrum power in the higher degrees, but it does provide high accuracy in the long wavelengths. Fig. 4.4 depicts the degree- and error-degree variances for the RBF shape in terms of potentials. Fig. 4.5 also shows the RBF kernel that resulted from error-degree variance.

The spline kernel has been developed to reflect the expected unknown gravity field characteristics, because the maximum degree employed for the regional recovery corresponds to a spherical harmonic expansion of up to a maximum degree N_{max}. The expansion has been truncated at degree $N_{max} = 120$ for this study. The spline kernels should be adapted to the spectral range of the gravity field features to be computed when using splines as space localizing basis functions. The shape of the basis function typically reaches its highest value at the nodal points Q_i and oscillates as the distance from the center increases, as represented by the spherical distance from these nodal points (i.e given on the graph as an opening angle with degree unit). The basis function never becomes zero if it is not defined as a band-limited function. The basis function narrows as the degree of expansion increases. From a spectrum standpoint, this means that larger basis functions are better for representing lower frequencies, whereas narrow basis functions are better for representing higher frequencies (Wittwer, 2009). A larger degree of expansion is required to restore finer structures of the gravitational field.

The scaling coefficients a_i are the desired quantities to be obtained inside the least-squares adjustment for the representation of the gravity field signal in terms of RBFs, where i denotes the number of unknown weights.

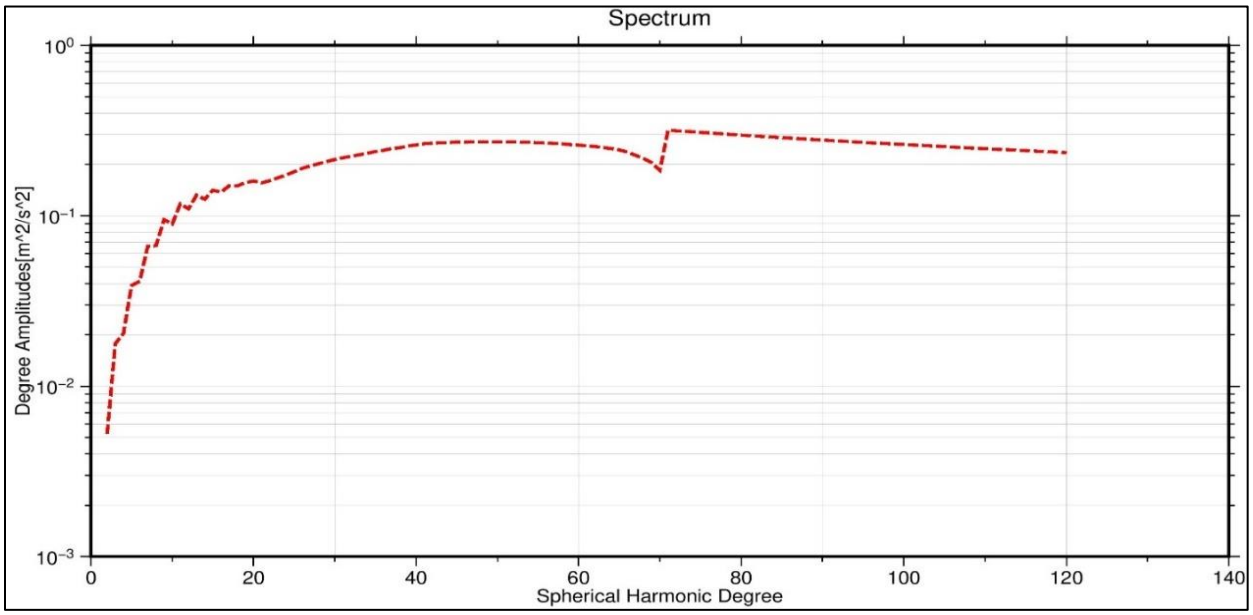

Figure 4.4 Degree variances for the spherical harmonic expansion.

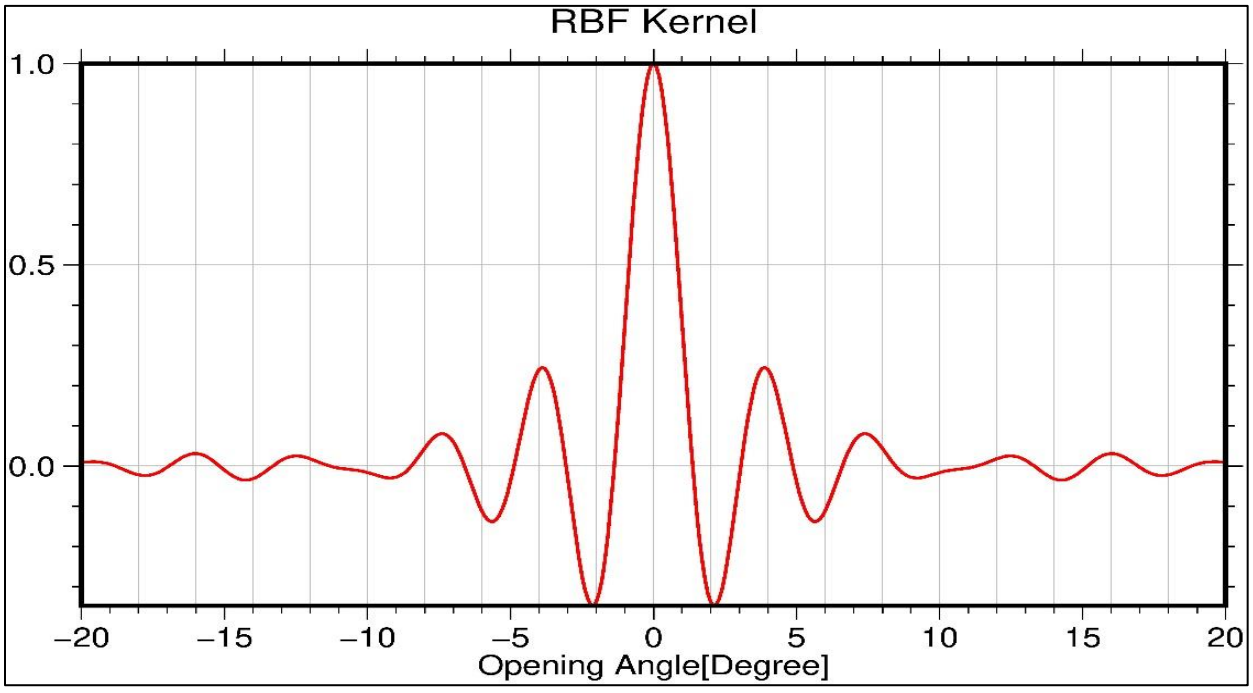

Figure 4.5 Normalized RBF kernel

Chapter Five

Result and Discussion

5.1 Result

5.1.1 One Month Solution

Regional solutions are determined as refinements to a global gravity field, as indicated in Chapter one. The global reference field is generally represented by spherical harmonics, whereas the residual gravity field is modeled using space localizing splines.

Only satellite data over the study area was utilized to recover the regional gravity field. Gravity field parameters defined in an additional strip around the study area must be taken into account to avoid geographical truncation effects at the study area boundaries; in most cases, a strip of 10° is sufficient (Mayer-Gürr et al., 2006). The nodal points are arranged in a regular grid, with a mean distance between them of about 55 kilometers. This grid is made up of $0.5°x0.5°$ geographical grids. This brought the number of unknown parameters to be determined, 4480 totally for the study area.

The regional solution was derived using only one month of GRACE data, in this case, data gathered in January 2016. This RBF model computed from GRACE data is a static model, since the signal is assumed to be constant over the time span of the input data, i.e one month. The results were then compared to the global model Eigen-GL04C (Förste et al., 2008). This global model was constructed utilizing GRACE data of 2.5 years, as well as additional surface gravity data. The EGM96 (Lemoine et al., 1998) was used as a reference field up to degree n = 120, and the regional solution was calculated as refinements to this global reference field.

The integral equation technique was used to reconstruct the gravity field, as indicated thoroughly in the methodology part. The outcome of the above-mentioned setting is depicted in Fig. 5.1. The residual gravity field for the study area was recovered using a tailored regularization method, with a variance component estimation approach determining the regularization factor as well as the variance factors for the short arcs crossing the areas. Monthly solutions provide the benefit of allowing a solution derived from more data (and hence presumably better accuracy) to be used as a comparison and accuracy measurements to be calculated.

The residual gravity field over the study area has the statistical characteristics given in table 5.1.

Table 5.1 Statistics for residual gravity field (mGal)

Min	Max	Mean
−1.28	1.19	0

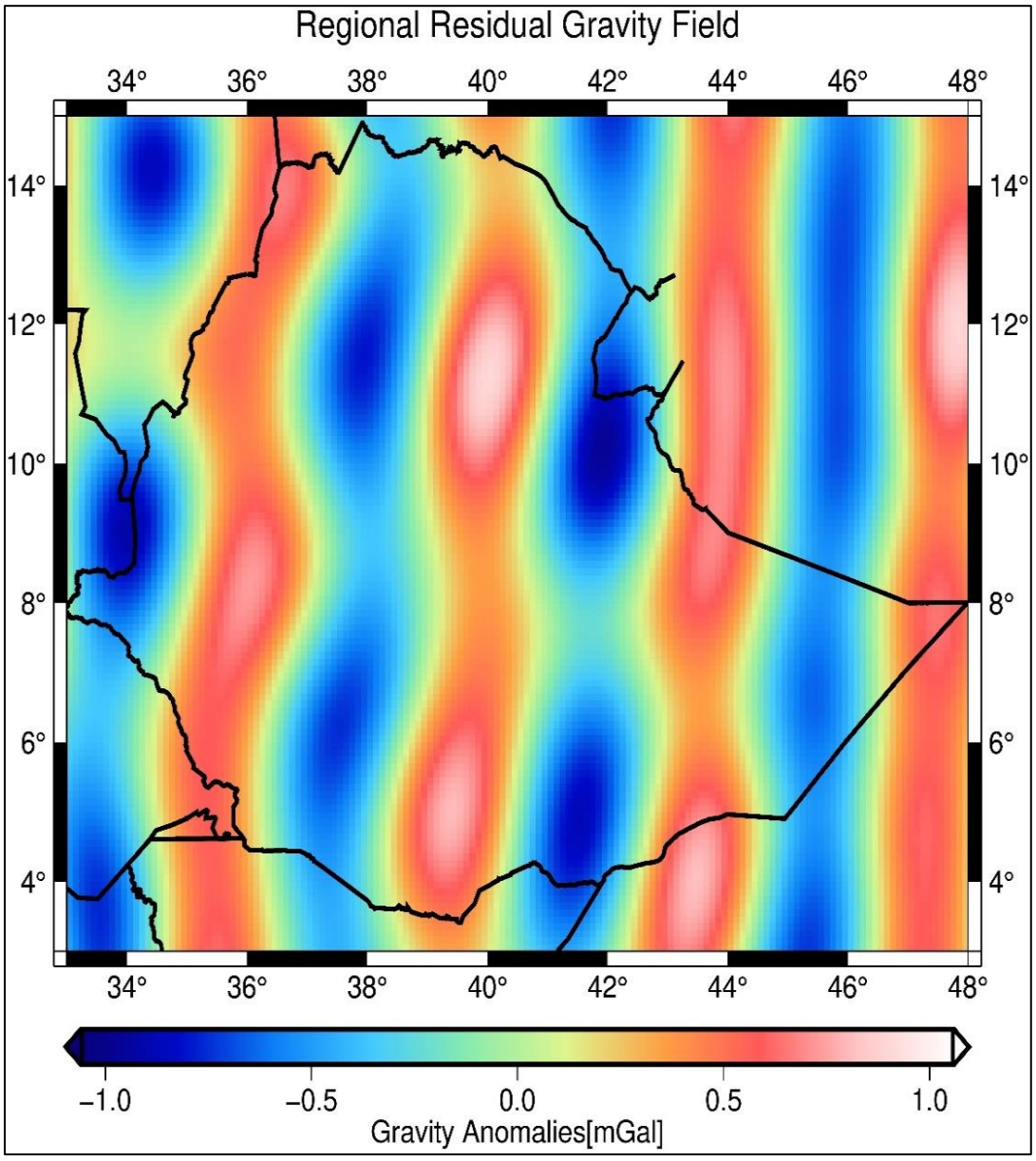

Figure 5.1 Regional Residual Gravity Field

5.1.2 Validation

This study employed the Eigen-GL04C global model (Förste et al., 2008), truncated to the same spherical harmonic degree as the solution, as an independent data set for evaluating both the global model EGM96 and the regional refinements over the study area.

Figures 5.2 shows the gravity anomaly calculated from the Global reference model (EGM96) before regional refinements and after refinement by spline functions.

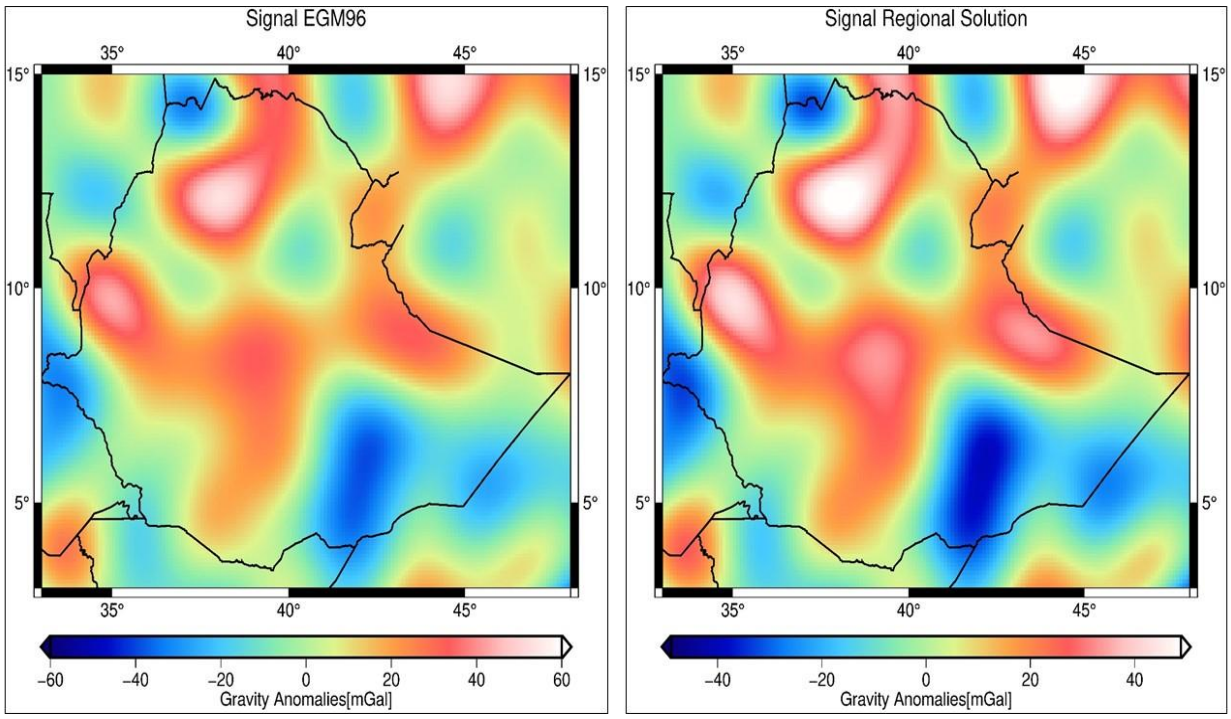

Figure 5.2 Gravity anomalies before refinement (left) and after regional refinement (right).

When compared to the globally averaged signal (see Fig. 5.2), the gravity field across the study area is smooth, and it has the potential to be improved by adapting the regularization to the local signal characteristics. The estimated gravity field for the global model EGM96 is shown in Fig. 5.2 (left), and the regional refinement from RBF modeling is shown in Fig. 5.2 (right). The regional model appears to have a lower noise level, as seen in Fig. 5.3 (right) and 5.3 (left), which show the differences between the two solutions to the Eigen-GL04C global model.

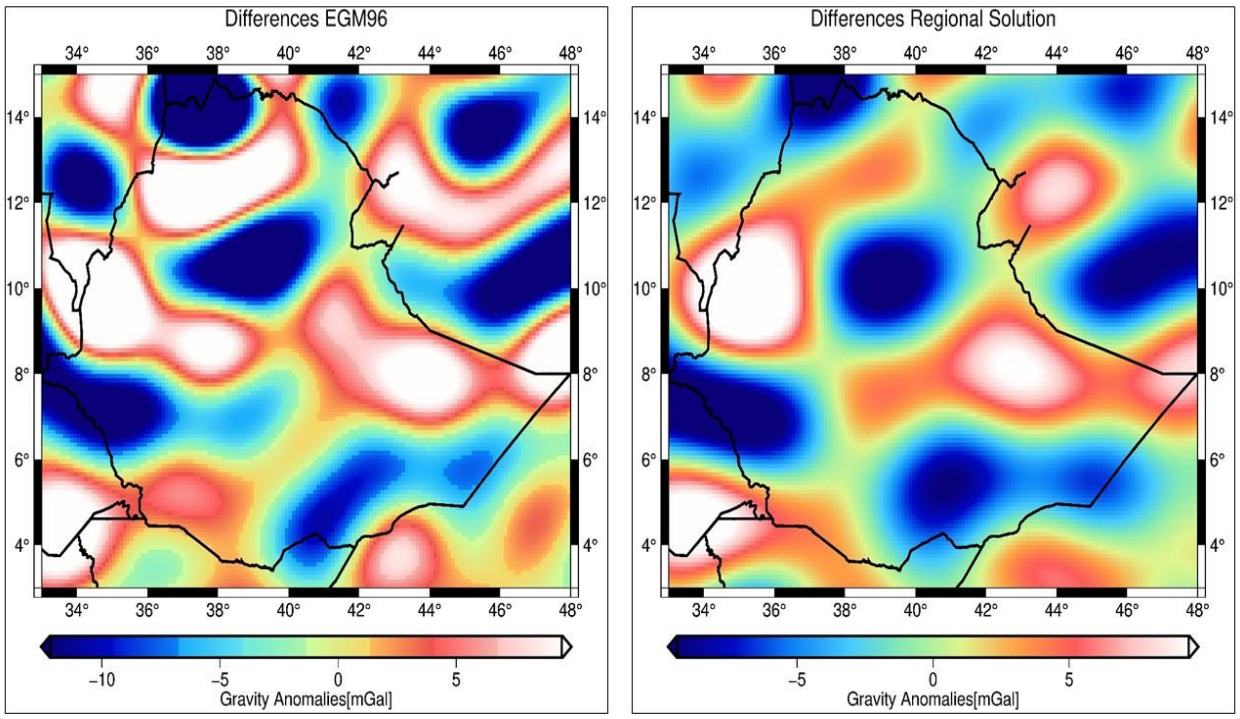

Figure 5.3 Difference signal EGM96 (left) and Regional solution (right)

The difference rms for the global model is $5.95 mGal$, whereas the regional refinement has an rms of $4.33 mGal$. This is equivalent to a 27.27 percent reduction in noise level. Table 1 shows the corresponding rms values in terms of geoid heights as well. The relative improvement attained by regional refinement is reported for both functionals.

Table 5.2 RMS in terms of gravity anomalies and geoid heights of the differences between global solution and regional with Eigen-GL04C

EGM96		**Regional**		**Improvement**	
$\Delta g(\boldsymbol{mGal})$	N(cm)	$\Delta g(mGal)$	N(cm)	$\Delta g(percent)$	$N(percent)$
5.95	**52.90**	**4.33**	**46.13**	**27.27**	**12.80**

5.2 Limitation of the Study

The present study strived with all possible efforts in including all necessary input data and processing steps. However, the study experiences certain limitations. One of the foremost challenges was the lack of adequate resources and limitations in the field of satellite data processing (i.e both in theory and practical knowledge), especially in the gravity recovery area. This restricted the amount of data used for processing and has affected the quality of some preprocessing steps. The second one was the absence of familiarity with the software used for the processing of all steps in this study about the working principles and the theoretical basis upon which the algorithm works. Nevertheless, this study provides a stepping stone for others who are interested in doing research in gravity recovery using satellite data over the study area.

5.3 Discussion

To recover the signal information contained in the satellite and sensor data to its full extent, it is reasonable to adapt the analysis technique according to the specific characteristics of the gravity signal present in distinct regions. The gravity field characteristics vary greatly in different geographical places, especially in the higher frequency part of the spectrum. These heterogeneities are caused by different topographical characteristics with rough gravity signals, such as those generated by mountainous areas or deep-sea tunnels, and smooth signal areas, such as those seen in parts of the open ocean (Eicker, 2008). There are distinct topographical zones in Ethiopia. With elevations ranging from 116 meters below sea level in the Danakil depression to over 4,600 meters in the mountainous highlands, it is a land of geographical contrasts. This study used RBFs as a representation. They are made up of the gravitational potential's degree variances, therefore they are supposed to reflect the frequency spectrum of the expected gravity field signal.

A study by (Eicker et al., 2014) presented a regional gravity retrieval technique that outperformed Spherical Harmonic(SH) modeling in a variety of case studies and when applied to the identical Goce1b data. This method for determining regional gravity fields from GOCE gradiometry uses radial basis functions to parameterize and allows for regional tailoring of regularization. From November 1, 2009, to July 1, 2010, 7.5 months of GOCE data were covered. To parametrize the same resolution as ITG-Goce02, the RBF was constructed up to degree $n = 240$.

Case studies for the Pacific Ocean, the area around the South Sandwich Trench in the Southern Atlantic, and the North Sea were done as part of the refining of the global GOCE only model ITG-Goce02. The results were evaluated against the EGM2008 global high-resolution gravity field model and altimetry data. When the results for the Pacific Ocean were compared to the EGM2008, the rms in terms of gravity anomaly improved from 4.11 $mGal$ to 2.03 $mGal$, and in terms of geoid height improved from $12.81cm$ to $6.89cm$, a 46 percent improvement.

In another study conducted by (Eshagh et al., 2018), they used the GOCE mission's in-orbit diagonal components of the gravitational tensor to recover gravity anomalies with a resolution of 1°x1° at sea level in Ethiopia. This study used good coverage of gravitational tensor data over the whole study area, which was collected for 9 months period from January to September 2013 with 3-second sampling. The TIM-R5 is limited to degree and order 200 to assess the quality of the recovered gravity anomalies. With an rms of about $4.1mGal$, the joint inversion of the tensors produces anomalies that are close to those of TIM-R5.

(Eicker et al., 2009) also calculated the regional refinement to the global gravity field model using one month of GRACE data. The comparison with the similar monthly solution of GFZ-RLO4 in SH by differencing with Eigen-GL04C revealed that the regional solution matches significantly better than SH model. The improvement quantified in terms of geoid height using rms as from $16.50cm$ to $9.26cm$.

This study attempted to model regional gravity field utilizing Grace1B data over the study area as a refinement calculation for EGM96 Global Gravity Model. This reference model was used to generate the shape coefficients for the RBFs by using its degree variances. The linear accelerometer data of the Grace1B was also calibrated using modelled non-gravitational accelerations. The out-come of the data processing by employing the regional refinement technique shows an improvement over SH modeling of global support. This improvement was calculated in terms of gravity anomaly and geoid height respectively. In case of gravity anomaly the difference with Eigen-GL04C became $4.33mGal$ from $5.95mGal$ and for geoid height from $52.90cm$ to $46.13cm$. This made the percentage of improvement 27.27% for gravity anomaly and 12.80% for geoid height respectively.

The geographical distribution of the radial basis function and the bandwidth of the radial basis function are two significant variables that define the quality of a gravity field model based on radial basis functions (Wittwer, 2009). Even though they are linked to the above two criteria, the amount of data also plays a significant role, as shown in the study (Eshagh et al., 2018), which identified a limited period of revolution and differences in processing methods between the solution and the model against which it is being validated as sources of quality degradation during comparison. The limitation of the data only for one month during this study had an effect on the quality during comparison as well as the maximum degree that can be recovered. Because as the data get denser, the maximum degree that is going to be derived increases and this makes the resolution finer.

In general, the study attempted to model the regional gravity field utilizing Grace1B data over the study area, and the refinement calculation showed an improvement over spherical harmonics (SH) modeling. The approach used is characterized by, the short-arc approach, which allows data to be used only in the region of interest, RBFs derived from the degree variances of the reference gravity field are used to estimate the gravity potential (as a residual to a reference SH model) and a regularized least-squares estimator, weighted by variance component estimation. When comparing the regional refinement method to SH modeling, the regional refinement technique reduces noise in areas with a smooth gravity field. Additional information can also be extracted in places with a rough gravity field.

Chapter Six
Conclusion and Recommendation

6.1 Conclusion

On the basis of GRACE mission satellite data, a method for regional refining of global gravity field models was used in this study. This method includes the creation of specially tailored space localizing basis functions, as well as their associated locations according to a suitable nodal point pattern, a functional model based on the satellite's orbit's short arcs, and regional customization of the analysis process. The shape coefficients of the basis functions were obtained using the degree variances of the reference field, and they were constructed using radial spline kernels. The basis functions in this method reflected the frequency characteristics of the gravity field to be represented.

The approach starts by selecting just satellite data from that geographic area, necessitating the employment of a functional model based on the satellite's orbit's short arcs. A functional model based on the solution of a Fredholm type integral equation was used to explain the analysis of satellite-to-satellite tracking data. The downward continuation process is another key part of the regional gravity field analysis. A regionally customized regularization was presented in this context, which assigns distinct regularization matrices to geographical locations with variable signal content. As a result, a global dampening of gravity field characteristics may be avoided since the tailored regularization value generated for each region can account for varying signal content. As a result, it was expected that more information could be extracted from provided data than could be extracted from directly computed global gravity field solutions.

In this study, an accelerometer calibration approach based entirely on non-gravitational force modeling is used. The calibration results are compared to non-gravitational modeled forces. With the relatively high residual in the along-track direction, it can be concluded that model-based calibration performance was poor in this direction compared to the other two directions because of drag domination in the along-track direction.

For the other two directions, cross-track and radial, the non-gravitational forces are mainly of radiative origin, and model-based calibration seems to be advantageous.

Only one month of January GRACE data was analyzed in this study. To show the performance of the regional refinement, a solution was derived from this one-month data and compared by differencing with EIGEN global model before and after refinement. The resultant regional model agreed better with the global model produced from a substantially bigger quantity of data than the regional refinement. In terms of gravitational anomaly, there was a 27.27 percent reduction in rms.

To summarize, it can be stated that, as proven by the result of this study, localized refining procedures may significantly enhance global models. It is preferable to identify signal information in the higher frequency part of the spectrum using locally customized analysis and modeling approaches.

6.2 Recommendations

It is expected that these findings have an impact on many applications. As the strength of the regional refinement approach, the current study aims at using the spatial distribution of the RBFs in response to the geographically variable signal characteristics only with the one-month data of GRACE. It is recommended that future studies will also use good preprocessed data and extension of the data span to cover more time. Well suited calibration approach for the along-track direction is among the factors which have a great contribution to the accuracy of the final results.

References

Baur O. and Sneeuw N. (2006). Slepian approach revisited: new studies to overcome the polar gap. *3rd International GOCE User Workshop, Frascati, Italy*.

Bentel K., Schmidt M. and Gerlach C. (2013). Different radial basis functions and their applicability for regional gravity field representation on the sphere. *GEM-International Journal on Geomathematics*, *4*(1), 67–96.

Bettadpur S. (2012). *GRACE 327–720, Gravity recovery and climate experiment, product specification document. Rev. 4.5*. CSR-GR-03-02, ftp://podaac. jpl. nasa. gov/allData/grace/docs/ProdSpecDoc_v4 ….

Bruns H. (1878). *Die Figur der Erde: Ein Beitrag zur europäischen Gradmessung*. P. Stankiewicz.

Case K., Kruizinga G. and Wu S.-C. (2010). *GRACE Level 1B Data Product User Handbook*.

Ditmar P., Kuznetsov V., Van der Sluijs A. A., Schrama E. and Klees R. (2006). 'DEOS_CHAMP-01C_70': a model of the Earth's gravity field computed from accelerations of the CHAMP satellite. *Journal of Geodesy*, *79*(10), 586–601.

Ebinger C., Ayele A., Keir D., Rowland J., Yirgu G., Wright T., Belachew M. and Hamling I. (2010). Length and timescales of rift faulting and magma intrusion: The Afar rifting cycle from 2005 to present. *Annual Review of Earth and Planetary Sciences*, *38*, 439–466.

Eicker A, Mayer-Gürr T. and Ilk K. H. (2004). A global CHAMP gravity field by merging of regional refinement patches. *Proceedings of the Joint CHAMP/GRACE Science Meeting. Www. Gfzpotsdam. de/Pb1/JCG/Eicker-Etal_jcg. Pdf*, *130*.

Eicker A, Schall J. and Kusche J. (2014). Regional gravity modelling from spaceborne data: case studies with GOCE. *Geophysical Journal International*, *196*(3), 1431–1440.

Eicker Annette. (2008). *Gravity field refinement by radial basis functions from in-situ satellite data*. Citeseer.

Eicker Annette, Mayer-Gürr T. and Ilk K.-H. (2009). Improved resolution of a GRACE gravity field model by regional refinements. In *Observing our Changing Earth* (pp. 99–104). Springer.

Eshagh M., Gedamu A. A., and Bedada T. B. (2018). Regional recovery of gravity anomaly from the inversion of diagonal components of GOCE gravitational tensor: a case study in Ethiopia. *Artificial Satellites*, *53*(2), 55–74.

Fengler M. J., Freeden W. and Michel V. (2004). The Kaiserslautern multiscale geopotential model SWITCH-03 from orbit perturbations of the satellite CHAMP and its comparison to the models EGM96, UCPH2002_02_0. 5, EIGEN-1s and EIGEN-2. *Geophysical Journal International*, *157*(2), 499–514.

Förste C., Schmidt R., Stubenvoll R., Flechtner F., Meyer U., König R., Neumayer H., Biancale R., Lemoine J.-M., and Bruinsma S. (2008). The GeoForschungsZentrum Potsdam/Groupe de Recherche de Geodesie Spatiale satellite-only and combined gravity field models: EIGEN-GL04S1 and EIGEN-GL04C. *Journal of Geodesy*, *82*(6), 331–346.

Freeden W. (1999). *Multiscale Modelling of Spaceborne Geodata Teubner Verlag Stuttgart*. Leipzig.

Freeden W., Gervens T. and Schreiner M. (1998). *Constructive Approximation on the Sphere with Applications to Geomathematics, Clarendon*. Oxford.

Furman T., Bryce J., Rooney T., Hanan B., Yirgu G. and Ayalew D. (2006). Heads and tails: 30 million years of the Afar plume. *Geological Society, London, Special Publications*, *259*(1), 95–119.

Gerlach C., Földvary L., Švehla D., Gruber T., Wermuth M., Sneeuw N., Frommknecht B., Oberndorfer H., Peters T. and Rothacher M. (2003). A CHAMP-only gravity field model from kinematic orbits using the energy integral. *Geophysical Research Letters*, *30*(20).

Grafarend I. E. W., Austen G. and Reubelt T. (2000). *Räumliche Schwerefeldanalyse aus semi-kontinuierlichen Ephemeriden niedrigfliegender GPS-vermessener Satelliten vom Typ CHAMP, GRACE und GOCE*.

Hadamard J. (1923). Lectures on cauchy's problem in linear partial differential equations, yale univ. *Press. New Haven*.

Han S. and Simons F. J. (2008). Spatiospectral localization of global geopotential fields from the Gravity Recovery and Climate Experiment (GRACE) reveals the coseismic gravity change owing to the 2004 Sumatra-Andaman earthquake. *Journal of Geophysical Research: Solid Earth*, *113*(B1).

Heiskanen W. A. and Moritz H. (1967). Physical Geodesy. WH Freeman and Company. *San Francisco, CA*.

Heitz S. and Stöcker-Meier E. (1994). *Grundlagen der physikalischen Geodäsie*. Dümmler.

Hofmann-Wellenhof B. and Moritz H. (2006). *Physical geodesy*. Springer Science & Business Media.

Holschneider M. (1995). Wavelets. *An Analysis Tool*.

Ilk K H. (1984). On the analysis of satellite to satellite tracking data. *Symposium on Space Techniques for Geodynamics, Volume 1*, *1*, 59–74.

Ilk Karl Heinz, Flury J., Rummel R., Schwintzer P., Bosch W., Haas C., Schröter J., Stammer D., Zahel W. and Miller H. (2005). *Mass transport and mass distribution in the Earth system*. Institut für Astronomische und Physikalische Geodäsie.

Ilk Karl Heinz, Löcher A., and Mayer-Gürr T. (2008). Do we need new gravity field recovery techniques for the new gravity field satellites? *VI Hotine-Marussi Symposium on Theoretical and Computational Geodesy*, 3–9.

Jäggi A., Hugentobler U. and Beutler G. (2006). Pseudo-stochastic orbit modeling techniques for low-Earth orbiters. *Journal of Geodesy*, *80*(1), 47–60.

Keir D., Hamling I. J., Ayele A., Calais E., Ebinger C., Wright T. J., Jacques E., Mohamed K., Hammond J. O. S. and Belachew M. (2009). Evidence for focused magmatic accretion at segment centers from lateral dike injections captured beneath the Red Sea rift in Afar.

Geology, *37*(1), 59–62.

Keller W. (2008). *Wavelets in geodesy and geodynamics*. de Gruyter.

Kim J. (2000). *Simulation study of a low-low satellite-to-satellite tracking mission*. The University of Texas at Austin.

Kirschner M., Montenbruck O. and Bettadpur S. (2001). Flight dynamics aspects of the GRACE formation flying. *2nd International Workshop on Satellite Constellations and Formation Flying*, 19–20.

Koch K-R and Kusche J. (2002). Regularization of geopotential determination from satellite data by variance components. *Journal of Geodesy*, *76*(5), 259–268.

Koch Karl-Rudolf. (1999). *Parameter estimation and hypothesis testing in linear models*. Springer Science & Business Media.

Kvas A., Behzadpour S., Ellmer M., Klinger B., Strasser S., Zehentner N. and Mayer-Gürr T. (2019). ITSG-Grace2018: Overview and evaluation of a new GRACE-only gravity field time series. *Journal of Geophysical Research: Solid Earth*, *124*(8), 9332–9344.

Landau H. J. and Pollak H. O. (1962). Prolate spheroidal wave functions, fourier analysis and uncertainty—III: the dimension of the space of essentially time-and band-limited signals. *Bell System Technical Journal*, *41*(4), 1295–1336.

Lemoine F. G., Kenyon S. C., Factor J. K., Trimmer R. G., Pavlis N. K., Chinn D. S., Cox C. M., Klosko S. M., Luthcke S. B. and Torrence M. H. (1998). *The development of the joint NASA GSFC and the National Imagery and Mapping Agency (NIMA) geopotential model EGM96*.

Löcher A. and Ilk K. H. (2007). A validation procedure for satellite orbits and force function models based on a new balance equation approach. *Dynamic Planet*, 280–287.

Mayer-Gürr T., Eicker A. and Ilk K. H. (2006). Gravity field recovery from GRACE-SST data of short arcs. In *Observation of the earth system from space* (pp. 131–148). Springer.

Mayer-Gürr T., Ilk K.-H., Eicker A. and Feuchtinger M. (2005). ITG-CHAMP01: a CHAMP gravity field model from short kinematic arcs over a one-year observation period. *Journal of Geodesy*, *78*(7), 462–480.

Moritz H. (1980a). Advanced physical geodesy. *Advances in Planetary Geology*.

Moritz H. (1980b). Geodetic reference system 1980. *Bulletin Géodésique*, *54*(3), 395–405.

Muller P. M., and Sjogren W. L. (1968). Mascons: Lunar mass concentrations. *Science*, *161*(3842), 680–684.

Naeimi M. (2013). *Inversion of satellite gravity data using spherical radial base functions*. Fachrichtung Geodäsie und Geoinformatik der Leibniz-Univ.

Phillips D. L. (1962). A technique for the numerical solution of certain integral equations of the first kind. *Journal of the ACM (JACM)*, *9*(1), 84–97.

Reigber C. (1969). *Zur Bestimmung des Gravitationsfeldes der Erde aus Satellitenbeobachtungen*. Institut für Astronomische und Physikalische Geodäsie.

Reubelt T, Austen G. and Grafarend E. W. (2003). Harmonic analysis of the Earth's gravitational field by means of semi-continuous ephemerides of a low Earth orbiting GPS-tracked satellite. Case study: CHAMP. *Journal of Geodesy*, *77*(5), 257–278.

Reubelt Tilo, Götzelmann M. and Grafarend E. W. (2006). Harmonic analysis of the earth's gravitational field from kinematic CHAMP orbits based on numerically derived satellite accelerations. In *Observation of the earth system from space* (pp. 27–42). Springer.

Rowlands D. D., Luthcke S. B., Klosko S. M., Lemoine F. G. R., Chinn D. S., McCarthy J. J., Cox C. M. and Anderson O. B. (2005). Resolving mass flux at high spatial and temporal resolution using GRACE intersatellite measurements. *Geophysical Research Letters*, *32*(4).

Schmidt M. (2001). *Grundprinzipien der Wavelet-Analyse und Anwendungen in der Geodäsie*.

Schmidt M., Fengler M., Mayer-Gürr T., Eicker A., Kusche J., Sánchez L. and Han S.-C. (2007). Regional gravity modeling in terms of spherical base functions. *Journal of Geodesy*, *81*(1), 17–38.

Schmidt R. (2007). Zur Bestimmung des cm-Geoids und dessen zeitlicher Variationen mit GRACE. *Scientific Technical Report/Geoforschungszentrum Potsdam*.

Schneider M. (1968). *A General Method of Orbit Determination by M. Schneider*. Royal Aircraft Establishment.

Schneider M. and Reigber C. (1970). On the Determination of field parameters using a generalized Fourier-Analysis. In *Dynamics of Satellites (1969)* (pp. 181–188). Springer.

Tapley B. D. and Reigber C. (2001). The GRACE mission: status and future plans. *AGU Fall Meeting Abstracts*, *2001*, G41C-02.

Tapley B., Ries J., Bettadpur S., Chambers D., Cheng M., Condi F., Gunter B., Kang Z., Nagel P. and Pastor R. (2005). GGM02–An improved Earth gravity field model from GRACE. *Journal of Geodesy*, *79*(8), 467–478.

Thalhammer M., Rummel R. and Ilk K. H. (1995). *Refined method for the regional recovery from GPS-SST and SGG*. Institut für Astronomische und Physikalische Geodäsie.

Thomas J. B. (1999). *An analysis of gravity-field estimation based on intersatellite dual-1-way biased ranging*. JET PROPULSION LAB PASADENA CA.

Tikhonov A. N. (1963). On the solution of ill-posed problems and the method of regularization. *Doklady Akademii Nauk*, *151*(3), 501–504.

Touboul P., Foulon B. and Willemenot E. (1999). Electrostatic space accelerometers for present and future missions. *Acta Astronautica*, *45*(10), 605–617.

Van Helleputte T., Doornbos E. and Visser P. (2009). CHAMP and GRACE accelerometer calibration by GPS-based orbit determination. *Advances in Space Research*, *43*(12), 1890–1896.

Wittwer T. (2009). Regional gravity field modelling with radial basis functions. *PUBLICATIONS ON GEODESY 72*.

Wolfenden E., Ebinger C., Yirgu G., Deino A. and Ayalew D. (2004). Evolution of the northern Main Ethiopian rift: birth of a triple junction. *Earth and Planetary Science Letters*, *224*(1–2), 213–228.

Wöske F., Kato T., Rievers B. and List M. (2019). GRACE accelerometer calibration by high precision non-gravitational force modeling. *Advances in Space Research*, *63*(3), 1318–1335.

Zehentner N. and Mayer-Gürr T. (2016). Precise orbit determination based on raw GPS measurements. *Journal of Geodesy*, *90*(3), 275–286.